

Hot Degenerates in the MCT Survey. III. A Sample of White Dwarf Stars in the Southern Hemisphere

P. Bergeron¹, F. Wesemael¹, G. Fontaine¹, R. Lamontagne¹, S. Demers¹, A. Bédard

Département de Physique, Université de Montréal, Montréal, Québec H3C 3J7, Canada
bergeron, lamont, demers, bedard@astro.umontreal.ca

M.-J. Gingras

Department of Physics and Astronomy, University of Waterloo, Waterloo, ON N2L 3G1,
Canada
m3gingras@uwaterloo.ca

S. Blouin

Los Alamos National Laboratory, Los Alamos, NM 87545, USA
sblouin@lanl.gov

M.J. Irwin¹

Royal Greenwich Observatory, Madingley Road, Cambridge, CB3 0EZ,
United Kingdom
mike@ast.cam.ac.uk

S.O. Kepler¹

Instituto de Física, Universidade Federal do Rio Grande do Sul, RS, Brazil
kepler@if.ufrgs.br

ABSTRACT

We present optical spectra of 144 white dwarfs detected in the Montreal-Cambridge-Tololo (MCT) colorimetric survey, including 120 DA, 12 DB, 4 DO, 1 DQ, and 7 DC stars. We also perform a model atmosphere analysis of all objects in our sample using the so-called spectroscopic technique, or the photometric technique in the case of DC white dwarfs. The main objective of this paper is to contribute to the ongoing effort of confirming spectroscopically all white dwarf candidates in the *Gaia* survey, in particular in the southern hemisphere. All our spectra are made available in the Montreal White Dwarf Database.

¹Visiting Astronomer, Cerro Tololo Interamerican Observatory, National Optical Astronomical Observatories, which is operated by AURA, Inc., under contract with the National Science Foundation.

1. Introduction

Large-scale colorimetric surveys are an important source of new hot subluminoous objects that can form the basis of many different types of investigations. For instance, the Palomar-Green (PG) survey (Green et al. 1986) has yielded a complete sample of white dwarfs from which the luminosity function of hot white dwarfs could be derived (see Liebert et al. 2005 for DA stars, and Bergeron et al. 2011 for DB stars). In addition, the PG survey increased considerably the number of objects in some sparsely populated classes (e.g., the DBA stars), as well as revealed the existence of entirely new kinds of objects (e.g., the very hot PG 1159 stars). The PG yield of subluminoous objects reawakened interest in colorimetric surveys, which have a long and distinguished history (Humason & Zwicky 1947; Feige 1958; Haro & Luyten 1962; Lanning 1973) in white dwarf astronomy. The following years have witnessed a flurry of activity in this area, with at least four analogs of the PG survey proceeding concurrently: the Kiso survey (Noguchi et al. 1980; Kondo et al. 1984); the Montreal-Cambridge-Tololo (MCT) survey (Demers et al. 1986); the Edinburgh-Cape survey (Stobie et al. 1987, 1992, 1997); and the Homogeneous Bright Quasars Survey, a Key Project carried out at ESO (Gemmo et al. 1993, 1995, see also Cristiani et al. 1995). At the same time, the yield of new degenerates identified in objective-prism surveys like the Hamburg/ESO and Hamburg Quasar Surveys (Reimers et al. 1996, 1998; Homeier et al. 1998) and the earlier Case Low-Dispersion Northern Sky Survey (Wagner et al. 1988) cannot be understated.

Of course, these old colorimetric surveys have now been completely superseded by the large Sloan Digital Sky Survey (SDSS), at least in the northern hemisphere, which identified well over 30,000 white dwarfs in the Data Release 14 (Kepler et al. 2019). In parallel, the *Gaia* Data Release 2 (Gaia Collaboration et al. 2018, hereafter GaiaHRD) has provided precise astrometric and photometric data for $\sim 260,000$ high-confidence white dwarf candidates (Gentile Fusillo et al. 2019). Although the spectroscopic follow-up of the *Gaia* sample is still in progress (see, e.g., Tremblay et al. 2020), many white dwarf candidates still require spectroscopic observations and confirmations, particularly in the southern hemisphere.

As part of this global effort, we decided to publish the spectroscopic results from the MCT survey, long overdue, and to make all of our spectra available in the Montreal White Dwarf Database¹ (MWDD; Dufour et al. 2017). We thus present in Section 2 a sample of 144 white dwarfs observed spectroscopically, several of which have previously been identified in other surveys, and discussed in the literature. These spectra are then analyzed in Section 3, and the global properties of our sample are discussed in Section 4.

¹<http://montrealwhitedwarfdatabase.org/>

2. Observations

2.1. The Photographic Survey

A detailed description of the photographic part of the MCT survey has been presented by Demers et al. (1986). In essence, doubly-exposed IIA O plates exposed through U and B filters were obtained at the CTIO Curtis Schmidt telescope. Exposure times are adjusted so as to yield comparable image sizes for objects with $(U - B) \sim -0.5$. The photographic plates were then measured using the Automatic Plate Measuring System (APM) at Cambridge (Kibblewhite et al. 1984). An internal magnitude scale was defined for both images, and the internal magnitudes were then transformed into B and U magnitudes either through published photoelectric sequences, or through calibrated CCD frames. As a general rule, we concentrated on the bluest objects, those with $(U - B) \leq -0.6$, although some redder objects, with $-0.6 \leq (U - B) \leq -0.4$ have been occasionally observed. All blue candidates were first visually inspected to weed out interlopers (e.g., U image contaminated by the B of a nearby star, stars near the edge of the plate, etc.).

Here we go one step further and take advantage of the *Gaia* photometric and astrometric data (EDR3; Gaia Collaboration et al. 2021; Lindegren et al. 2021) to confirm the nature of the objects identified in the MCT survey. In Figure 1 we present the M_G vs $(G_{BP} - G_{RP})$ color-magnitude diagram for the white dwarfs within 100 pc from the Sun identified in the MWDD, together with the white dwarfs identified in our survey. Different color symbols are used to distinguish H- and He-dominated atmospheres. Hot subdwarfs and other contaminants have been removed from the sample and can be made available upon request. Also shown are theoretical color sequences taken from our publicly available Web site². The observed sequence follows nicely the color track near $\sim 0.6 M_\odot$, with many hot white dwarfs reaching the Rayleigh-Jeans limit near $(G_{BP} - G_{RP}) \sim 0.5$, and several red objects whose colors are obviously contaminated by the presence of an M-dwarf companion are also present in the sample (see below). As expected, most white dwarfs in our sample are found at high effective temperatures ($T_{\text{eff}} \gtrsim 10,000$ K), although several cooler objects have also been uncovered.

2.2. Spectroscopic Observations

Follow-up observations of the blue candidates in the MCT survey have been secured, beginning as long ago as 1985. Most of the observations were obtained at the CTIO 1.5-m

²See <http://www.astro.umontreal.ca/~bergeron/CoolingModels>.

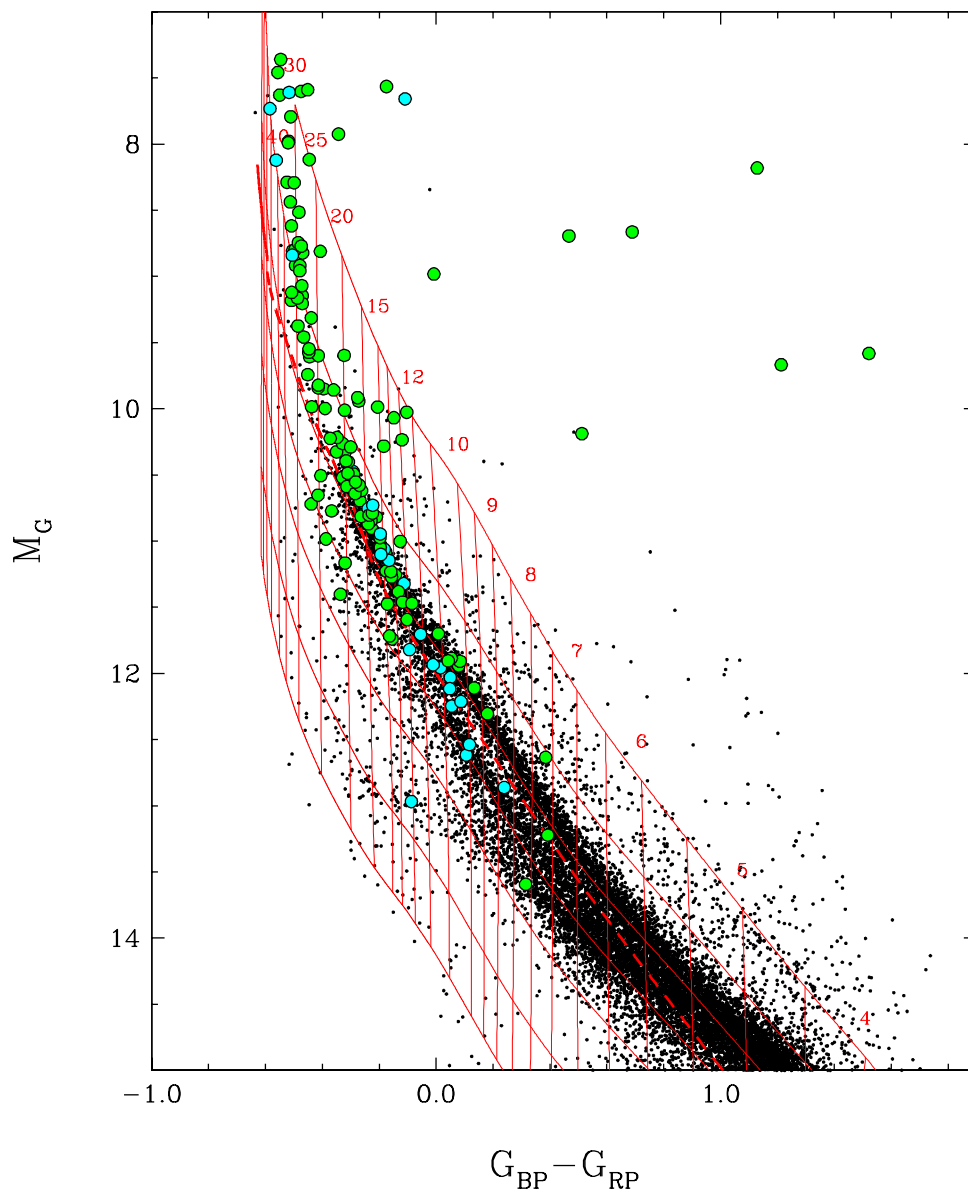


Fig. 1.— Gaia color-magnitude diagram for the 100 pc sample (small dots) drawn from the MWDD; the white dwarfs in the MCT survey with H and He atmospheres are indicated by filled green and cyan dots, respectively. Red solid lines show the cooling sequences for CO-core and pure H atmosphere white dwarf models with 0.2, 0.4, 0.6, 0.8, 1.0, 1.2, and 1.3 M_\odot (from top to bottom); the dashed line shows the sequence for 0.6 M_\odot pure He atmosphere models; T_{eff} values are indicated in units of 10^3 K.

and 4-m telescopes, with a variety of instrumental setups. Early runs at the 1.5-m made use of the UV SIT, RCA CCD no. 5, and GE CCD EPI no. 4, all in conjunction with the Cassegrain spectrograph. From 1988 to 1994, however, data has been gathered with the GEC CCD no. 10. For our last run (Nov. - Dec. 1995), the detector was upgraded to a thinned Loral 1200×400 device. The spectral resolution achieved is 6.5–13 Å. At the CTIO 4-m telescope, data were gathered with the RC spectrograph, Air Schmidt or Folded Schmidt camera, and either the GEC no. 11 or the TI no. 1 CCD with a resolution of 6–7 Å. In addition, two runs were secured in 1987 and 1989 at the Las Campanas 2.5-m telescope, equipped with a 2D Frutti detector, with a spectral resolution of 3 Å. Finally, a handful of spectra extending into the red were secured through service observing at the La Palma Observatory with the double spectrograph. Further details of our spectroscopic follow-up can be found in Lamontagne et al. (2000).

We provide in Table 1 the list of objects that will be analyzed in the next section, including the MCT name, the 1950 position, the photographic values of B_{ph} and $(U - B)_{\text{ph}}$, as well as the date, telescope, and spectral resolution (FWHM) for each spectrum.

The optical spectra for the 120 DA white dwarfs identified in our survey are displayed in Figure 2 in order of decreasing effective temperature. At the level of resolution of our spectroscopic observations, we could not identify any DAZ stars in our sample. Already obvious in this figure, however, is the contamination from an M-dwarf companion in several objects (see, e.g., MCT 0309–2730, MCT 2108–4310, MCT 2259–321).

Composite DA+M-dwarf systems that also have red spectra are displayed in Figure 3. From top to bottom: The blue spectrum of MCT 0208–1520 suggests the presence of additional features near MgH $\lambda 4780$. This is confirmed by the spectrum longward of 5500 Å, which rises steeply in the red, and which appears to match that of an M3 or M4 V companion. The blue spectrum of MCT 0309–2730 appears disturbed, and the presence of an unresolved companion is confirmed by the red spectrum, which matches that of an early-type M V star, perhaps M0 or M1. The blue spectrum of MCT 2313–3303 displayed in Figure 3 is clearly reminiscent of that of RE 2013+400 (Barstow et al. 1993) and RE 0720–318 (Barstow et al. 1995), where the cores of the Balmer lines are filled with reprocessed emission by the irradiated hemisphere of an M dwarf companion. In MCT 2313–3303, emission cores are seen in $H\beta$ and upward, while our red spectrum shows no emission at $H\alpha$. However, the latter was secured two days later than the blue spectrum, and the emission might be variable (as it is in RE 2013+400). The red coverage of the bottom object in Figure 3, MCT 0032–1313, is not as good as that of the two objects at the top of the figure, but it is sufficient to detect the presence of the M-dwarf companion.

The optical spectra for the 12 DB white dwarfs identified in our survey are displayed

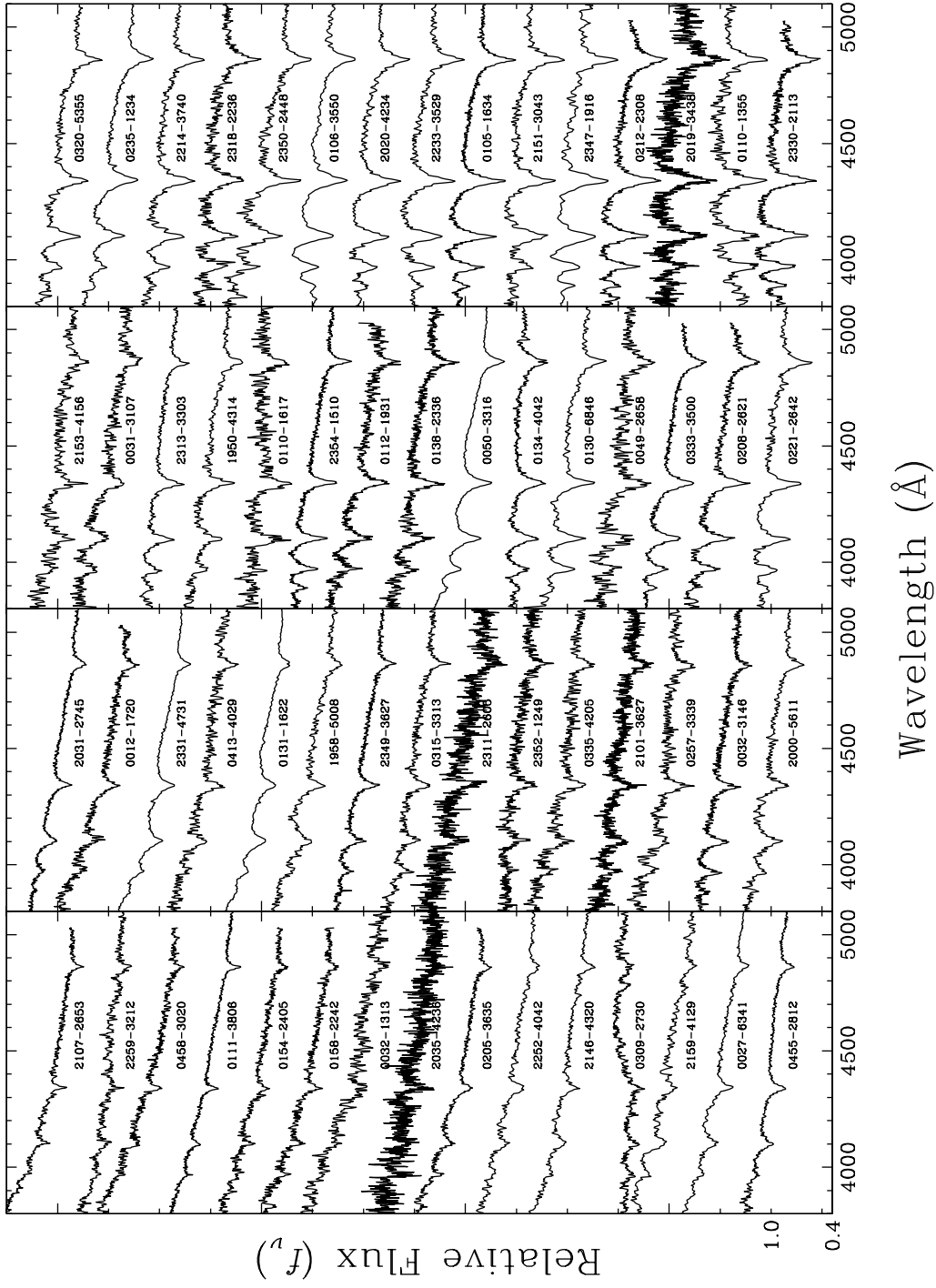


Fig. 2.— Optical (blue) spectra for our complete sample of DA stars. The spectra are normalized at 4500 \AA and shifted vertically from each other by a factor of 0.5 for clarity. The effective temperature decreases from upper left to bottom right.

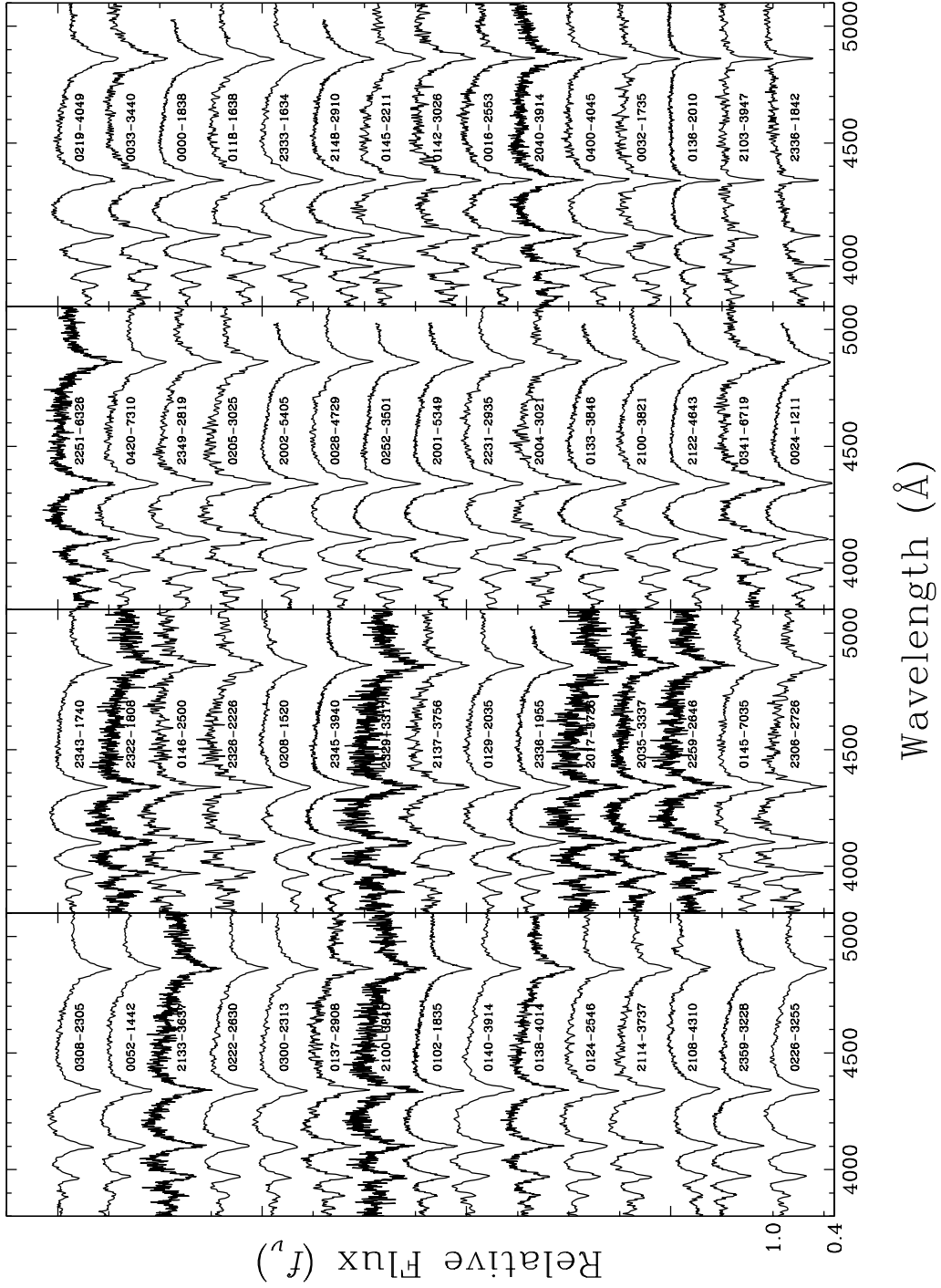


Fig. 2.— (Continued)

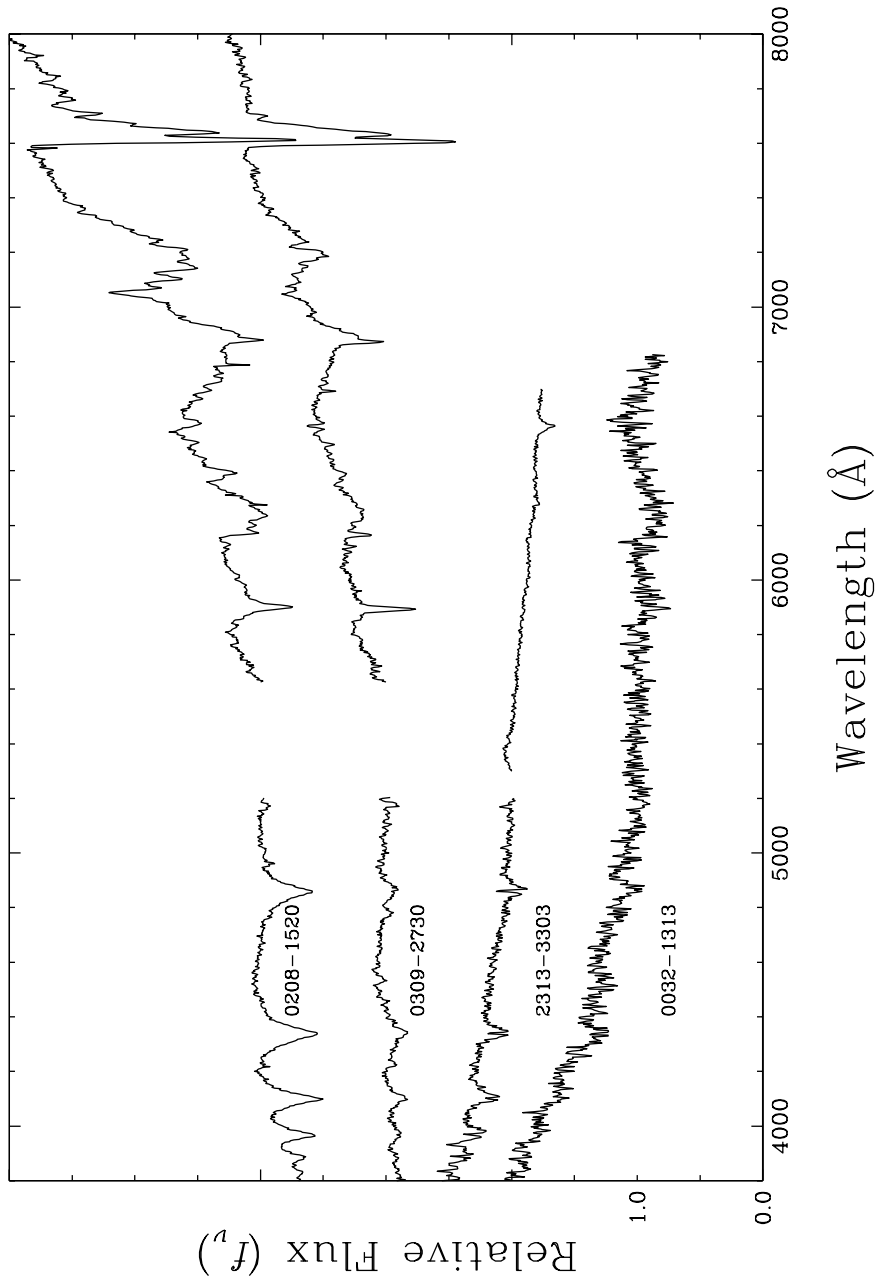


Fig. 3.— Composite spectra of DA+M-dwarf systems from Figure 2 for which red optical spectra are also available. The secondary star for 0208–1520 appears to be a M3 or M4 V companion, while for 0309–2730, the secondary star appears to be a M0 or M1 V companion.

in Figure 4 in order of decreasing effective temperature. In three of these objects (MCT 0442–3523, MCT 2033–2525, and MCT 2046–3016), $H\beta$ can be detected, which makes them DBA stars. Given our spectral coverage, we cannot exclude that some of the DB white dwarfs displayed here could also show an $H\alpha$ absorption feature.

The optical spectra for the 7 DC white dwarfs identified in our survey are displayed in Figure 5 in order of right ascension. Our photometric fits discussed below indicate that all these stars are hot enough to show hydrogen lines if they were DA stars, hence they must have He-dominated atmospheres. However, due to the lack of spectral coverage in the red, we cannot exclude that some of these objects could display a broad and shallow $H\alpha$ absorption feature, characteristic of the so-called He-rich DA white dwarfs (Rolland et al. 2018).

Finally, we show in Figure 6 optical spectra for white dwarfs in our sample with other spectral types. The top object, MCT 0130–1937, is a PG 1159 star already discussed at length in Demers et al. (1990), while the bottom two white dwarfs, MCT 0128–3846 and MCT 0453–2933, correspond to peculiar DAB stars analyzed in detail by Wesemael et al. (1994). The analysis of these 3 white dwarfs will not be repeated here. MCT 0101–1817, MCT 0501–2858, MCT 2148–2928, and MCT 2227–3246, are DO stars, while MCT 2137–3651 is the only DQ white dwarf identified in our sample. The spectroscopic analysis of these objects is described below.

Although not analyzed here, we show for completeness in Figure 7 the spectra of objects with strong emission lines. According to Simbad, MCT 0312–2246 and MCT 2115–3426 are cataclysmic variables, while MCT 2350–3908 is a nova.

3. Analysis of the Sample

In this section, we present a spectroscopic (or photometric) analysis of all the white dwarfs identified in the MCT survey (with the exception of three objects already analyzed elsewhere as mentioned above). Given the scope of our paper, we restrict ourselves to our own spectroscopic data, and thus, we do not attempt to obtain the most reliable atmospheric parameters for each object, nor will we cross-match our solutions with those already published in the literature.

The atmospheric parameters (T_{eff} and $\log g$) for the DA stars in our sample can be measured using the spectroscopic technique described in Bergeron et al. (1992), with various improvements discussed in Gianninas et al. (2011). Briefly, the normalized Balmer line profiles are compared with the predictions of detailed model atmospheres, properly convolved with the instrumentation profile, and the best fitting T_{eff} and $\log g$ values are obtained us-

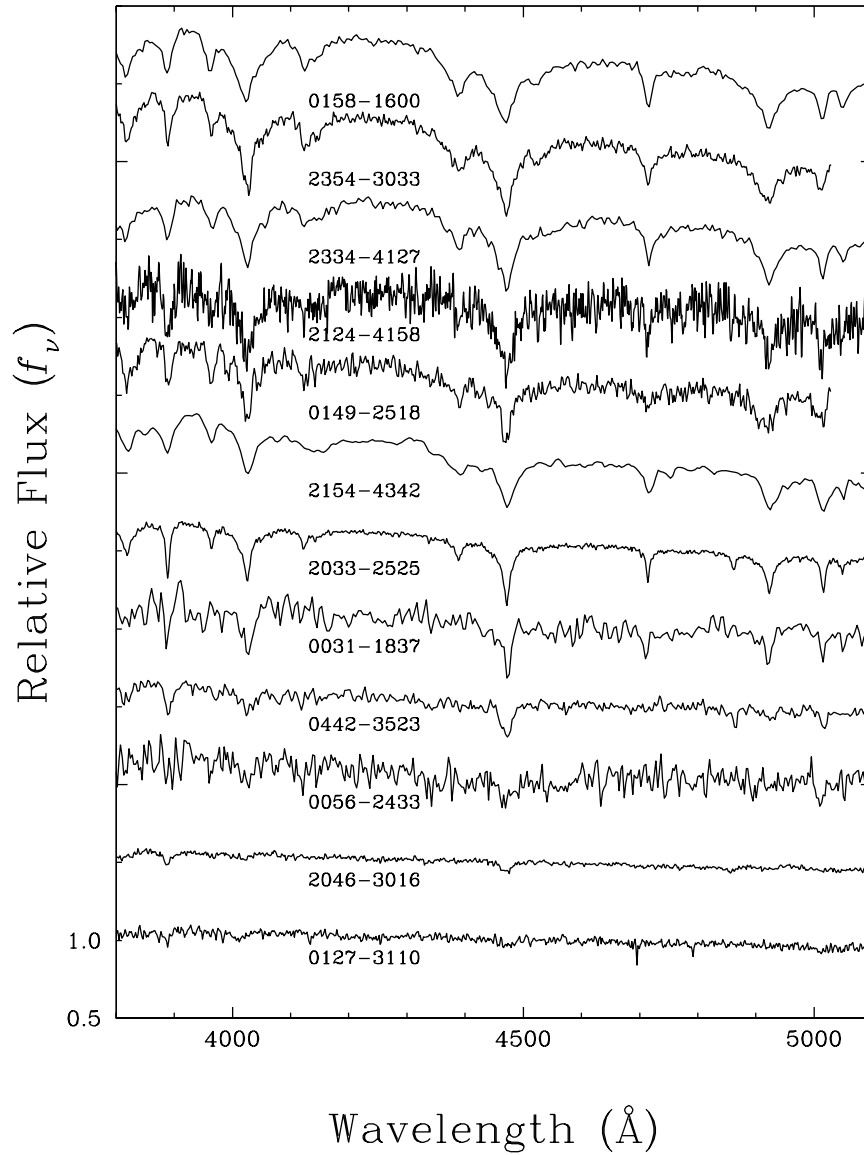


Fig. 4.— Optical (blue) spectra for our complete sample of DB and DBA stars. The spectra are normalized at 4500 \AA and shifted vertically from each other by a factor of 0.5 for clarity. The effective temperature decreases from top to bottom.

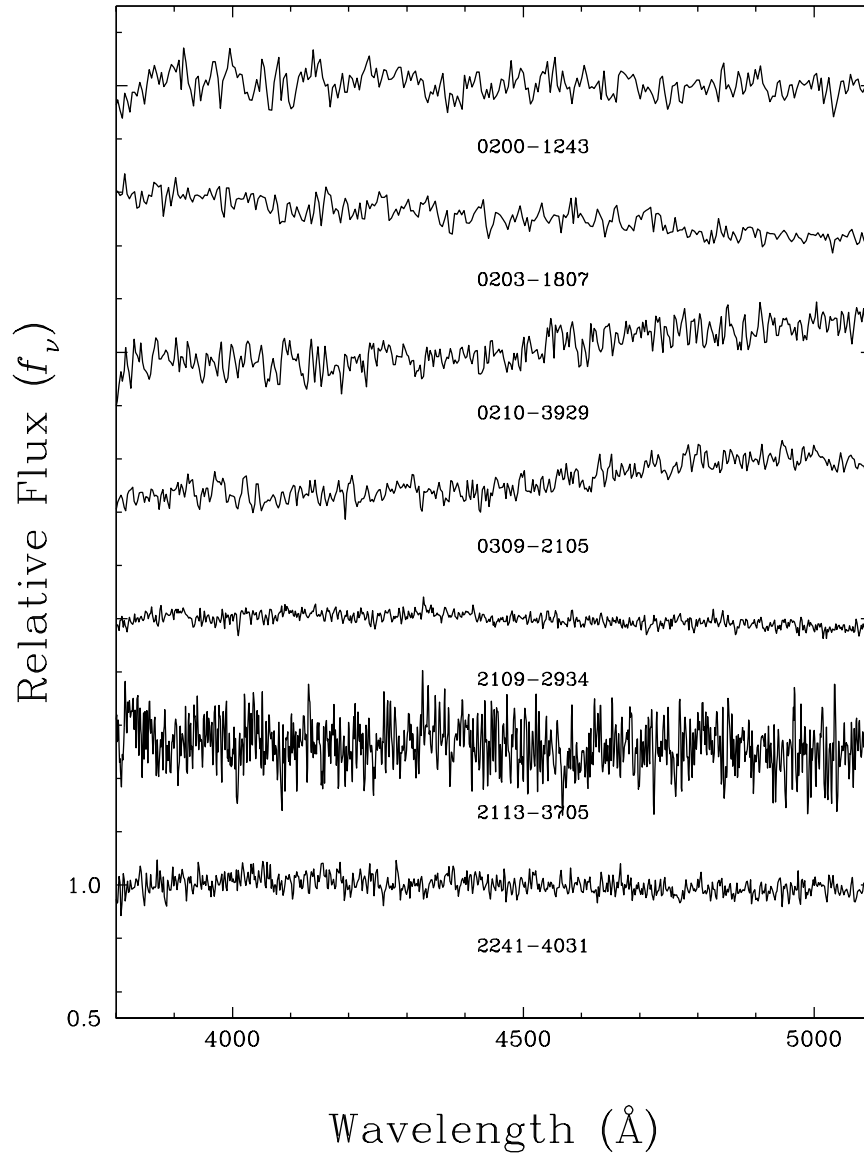


Fig. 5.— Optical (blue) spectra for our complete sample of DC stars, ordered by right ascension. The spectra are normalized at 4500 \AA and shifted vertically from each other by a factor of 0.5 for clarity.

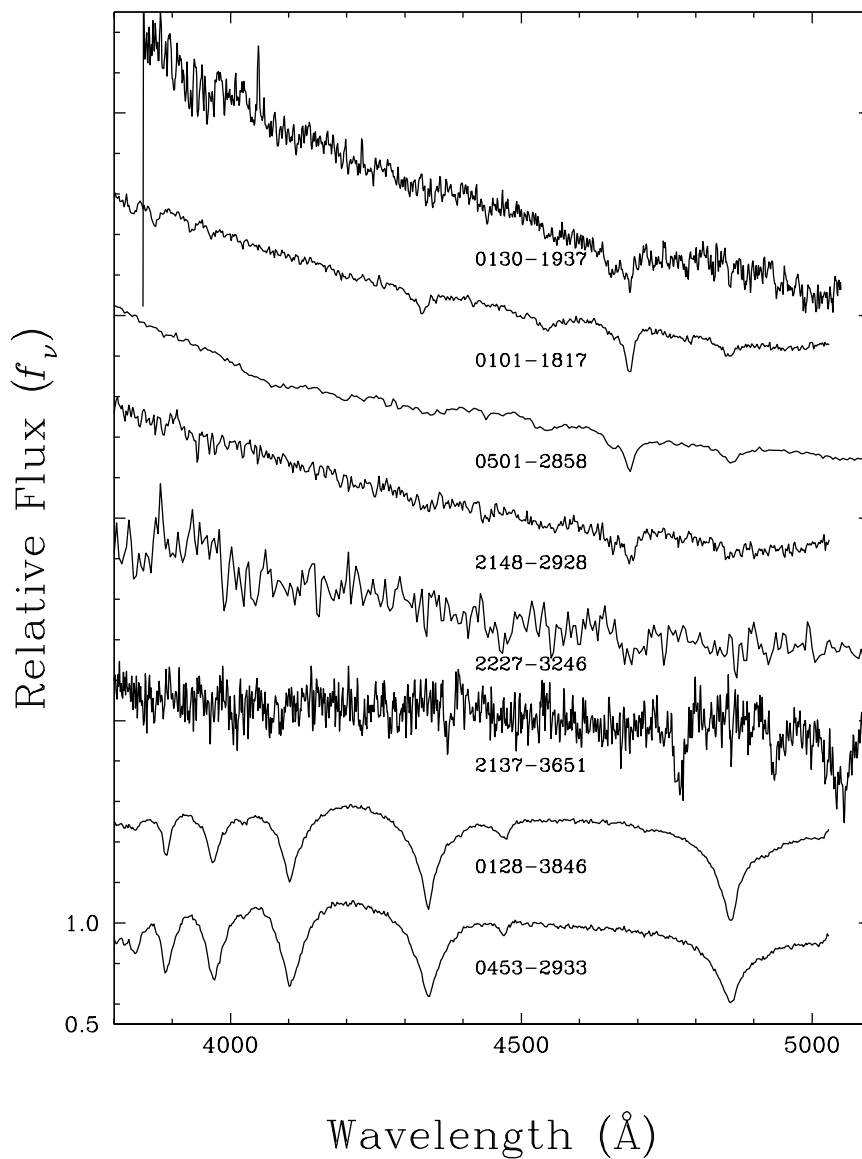


Fig. 6.— Optical (blue) spectra for miscellaneous white dwarfs in our sample; all spectra are normalized at 4500 Å and shifted vertically from each other by a factor of 0.5 for clarity. From top to bottom: MCT 0130–1937, a PG 1159 star already discussed in Demers et al. (1990); MCT 0101–1817, MCT 0501–2858, MCT 2148–2928, and MCT 2227–3246, four DO stars analyzed in this paper; MCT 2137–3651, the only DQ star in our sample, also analyzed in this paper; MCT 0128–3846 and MCT 0453–2933, two peculiar DAB stars analyzed in detail by Wesemael et al. (1994).

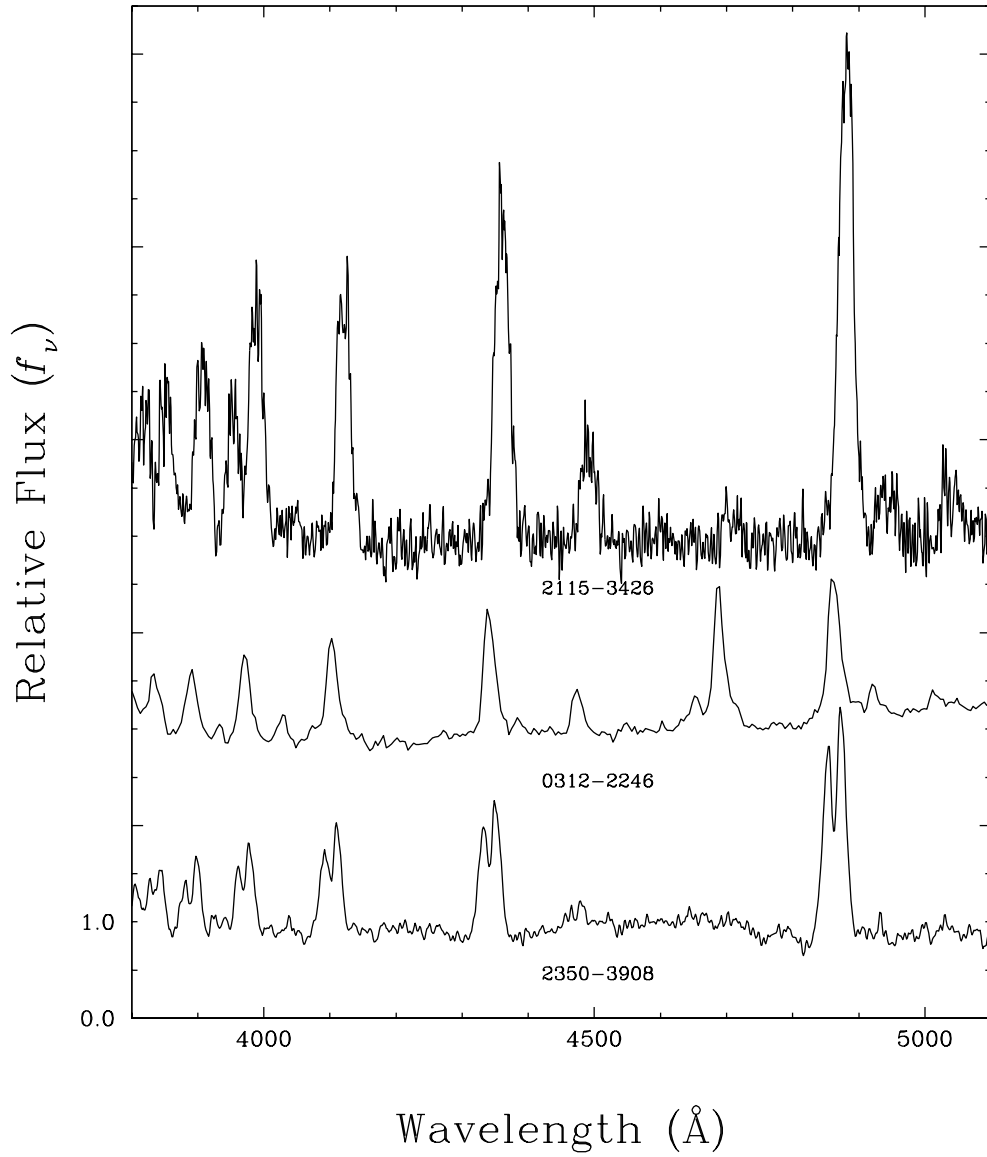


Fig. 7.— Optical (blue) spectra for the cataclysmic variables (MCT 0312–2246 and MCT 2115–3426) and the nova (MCT 2350–3908) identified in our survey.

ing a χ^2 minimization technique. The model atmospheres used here are similar to those presented in Tremblay et al. (2011a) and references therein, with the exception that the non-LTE models at high effective temperatures ($T_{\text{eff}} > 40,000$ K) have been replaced with those calculated by Bédard et al. (2020). Convective energy transport has been included in our calculations using the mixing-length theory with the $ML2/\alpha = 0.7$ convective efficiency. It is a well known problem that for DA stars close to the region where the Balmer lines reach their maximum strength ($T_{\text{eff}} \sim 13,000$ K), there exist two solutions, one of each side of this maximum (Bergeron et al. 1995). To distinguish between these cool and hot spectroscopic solutions, we rely on the photometric approach, described further below, to estimate T_{eff} using the *Gaia* astrometric and photometric data.

Our best fits for the DA stars in the MCT sample are displayed in Figure 8 in order of right ascension. The theoretical profiles shown in green are contaminated by the presence of an M-dwarf companion, and these lines are not included in the fit. Note that the 3D hydrodynamical T_{eff} and $\log g$ corrections of Tremblay et al. (2013) have been applied to the solutions displayed in these figures (see Section 4).

A similar approach can be used for the DB white dwarfs in our sample following the procedure and model atmospheres described in Bergeron et al. (2011), with improvements to the van der Waals broadening discussed in Genest-Beaulieu & Bergeron (2019). Here the full spectrum is normalized to a continuum set to unity, and there is one additional parameter to fit, the hydrogen-to-helium abundance ratio H/He (in number). Given the lack of spectral coverage in the red where $H\alpha$ is located, the value of H/He is determined by using $H\beta$, which is detected in only three objects in our sample; we simply assume a pure helium composition for the remaining objects. Our best fits for the DB and DBA white dwarfs in our sample are displayed in Figure 9 in order of decreasing effective temperature. The values of T_{eff} and $\log g$ are given in the figure, as well as $\log H/He$ in the case of DBA stars.

The four DO stars in our sample are fitted using the same method and model atmospheres as those described in detail in Bédard et al. (2020). A pure helium composition is assumed for all objects. Our best fits are displayed in Figure 10 in order of decreasing effective temperature, with the values of T_{eff} and $\log g$ given in the figure. Some of the fits displayed here show some problems discussed at length in Bédard et al., and we refer the reader to this paper for a full discussion. Briefly, MCT 0101–1817 and MCT 0501–2858 show abnormally broad and deep He II features that are poorly fitted by the models, thereby revealing the presence of a wind-fed circumstellar magnetosphere around these objects (Reindl et al. 2019, 2021). Note that MCT 0101–1817 also shows so-called ultra-high excitation lines in the blue, as also pointed out by Reindl et al. (2021). Finally, MCT 2148–2928 exhibits relatively strong C IV features and thus our pure-He models might not be appropriate for

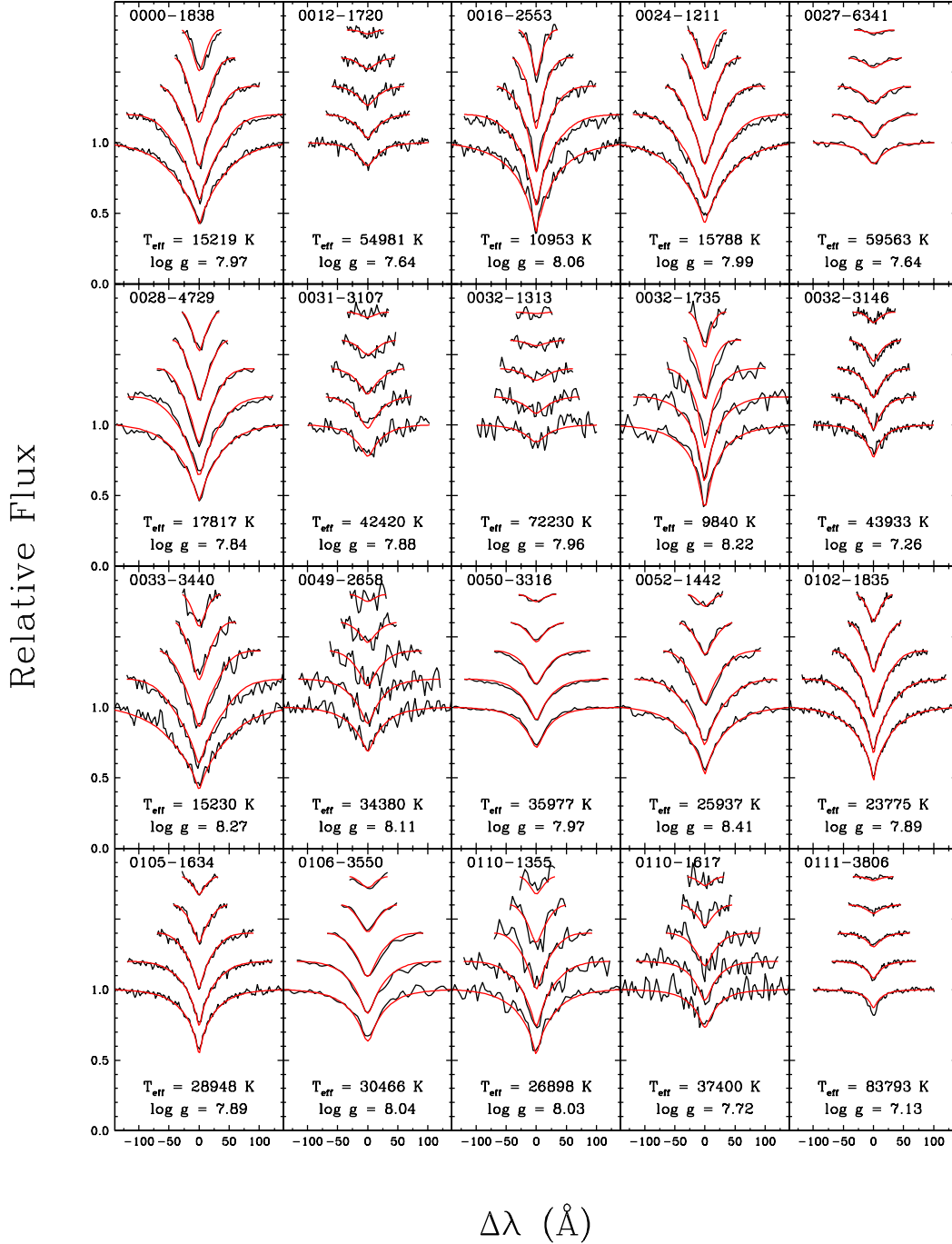


Fig. 8.— Model fits (red) to the individual Balmer line profiles (black) of the DA white dwarfs in our sample in order of right ascension. The lines range from $H\beta$ (bottom) to $H8$ (top), each offset by a factor of 0.2 (those shown in green are not included in the fit). The best-fit T_{eff} and $\log g$ values are indicated at the bottom of each panel; note that the 3D hydrodynamical T_{eff} and $\log g$ corrections have been applied to the solutions displayed here.)

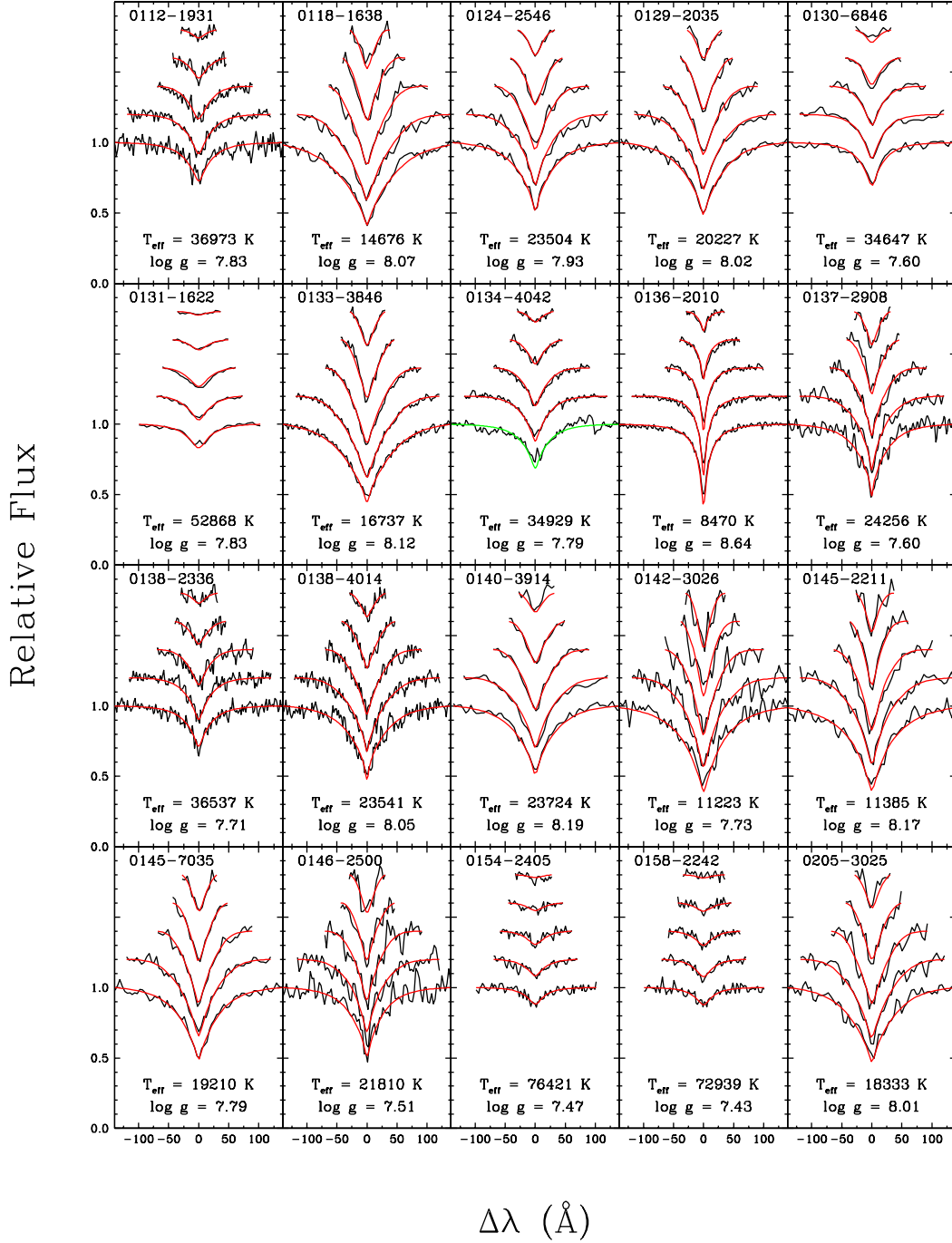


Fig. 8.— (Continued)

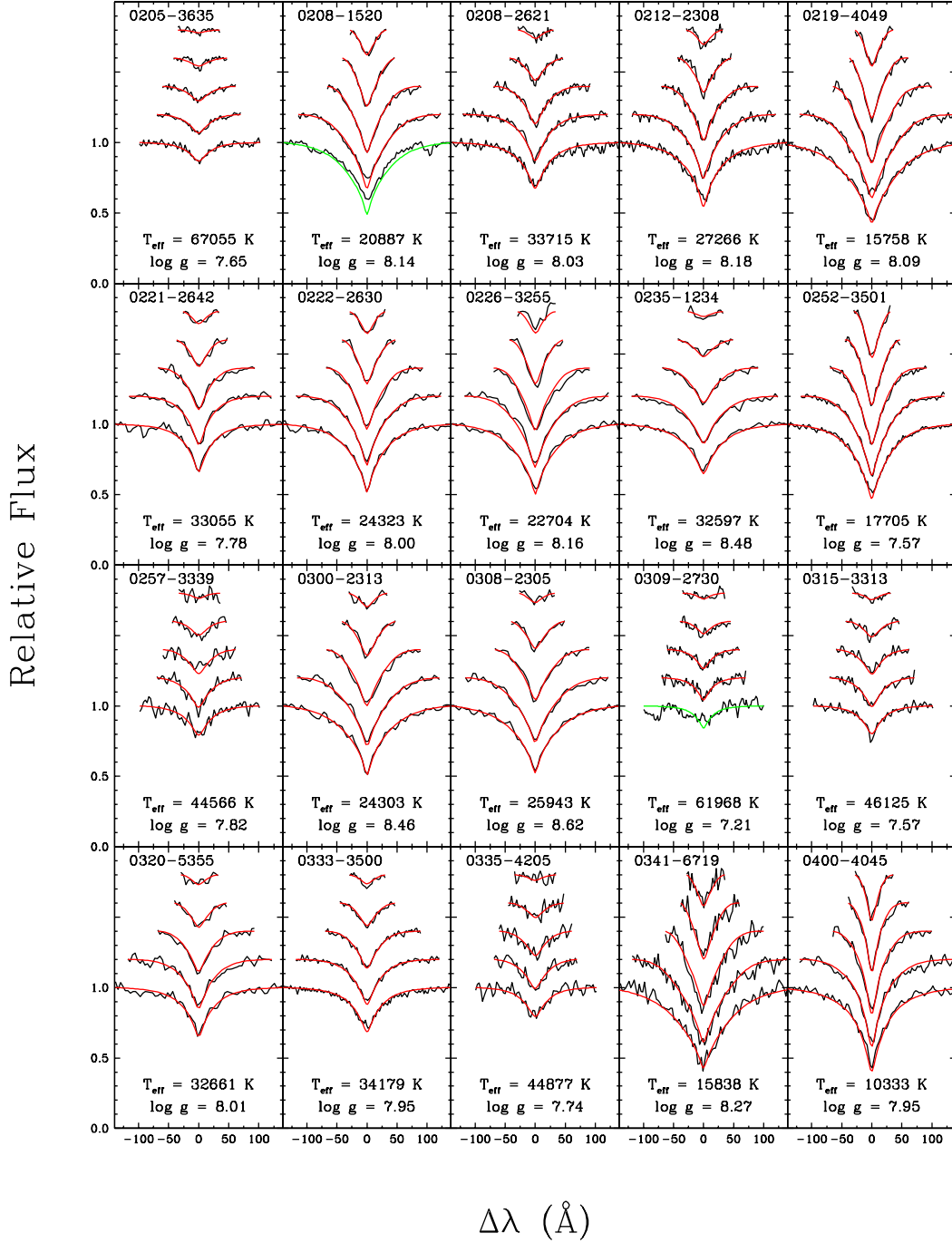


Fig. 8.— (Continued)

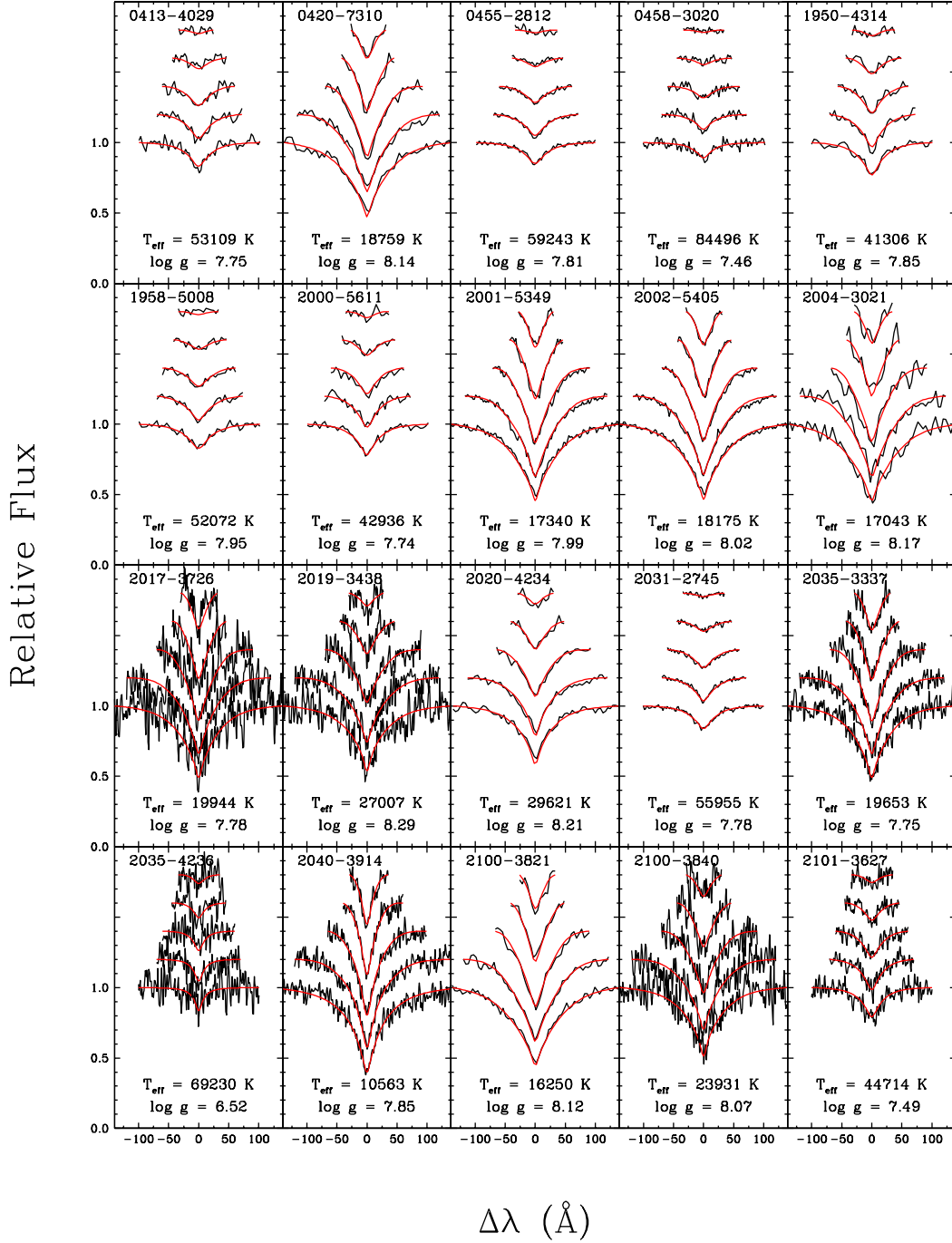


Fig. 8.— (Continued)

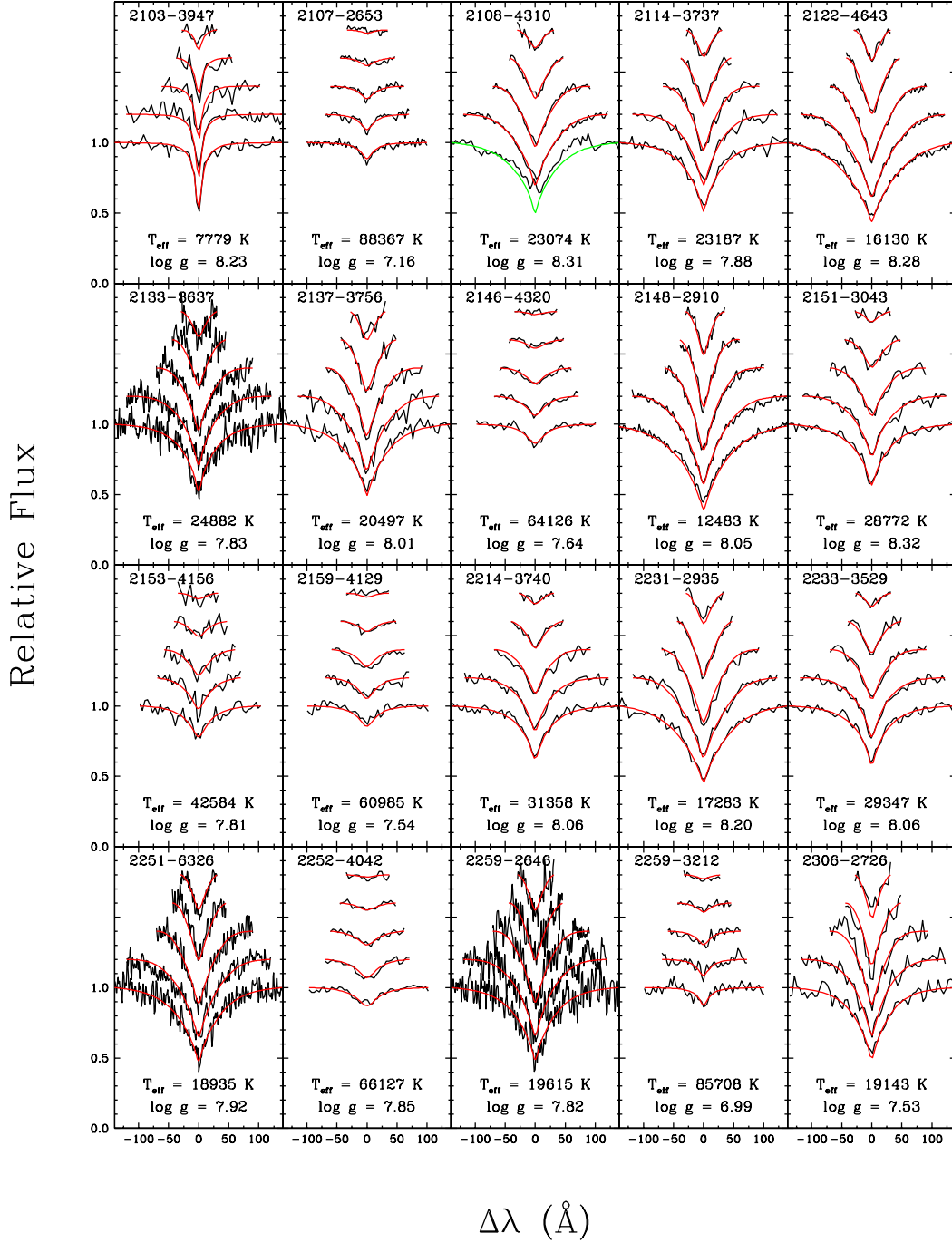


Fig. 8.— (Continued)

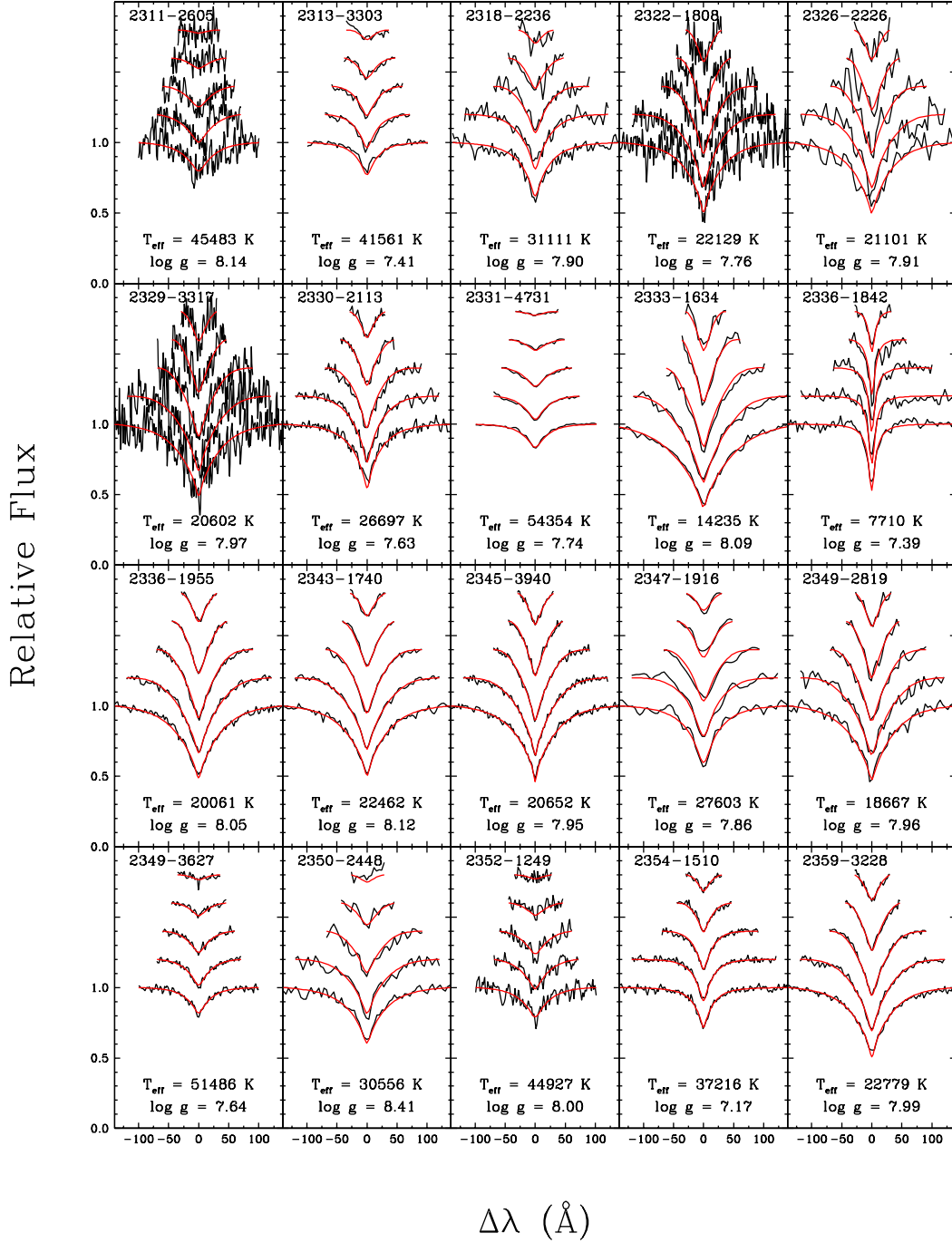


Fig. 8.— (Continued)

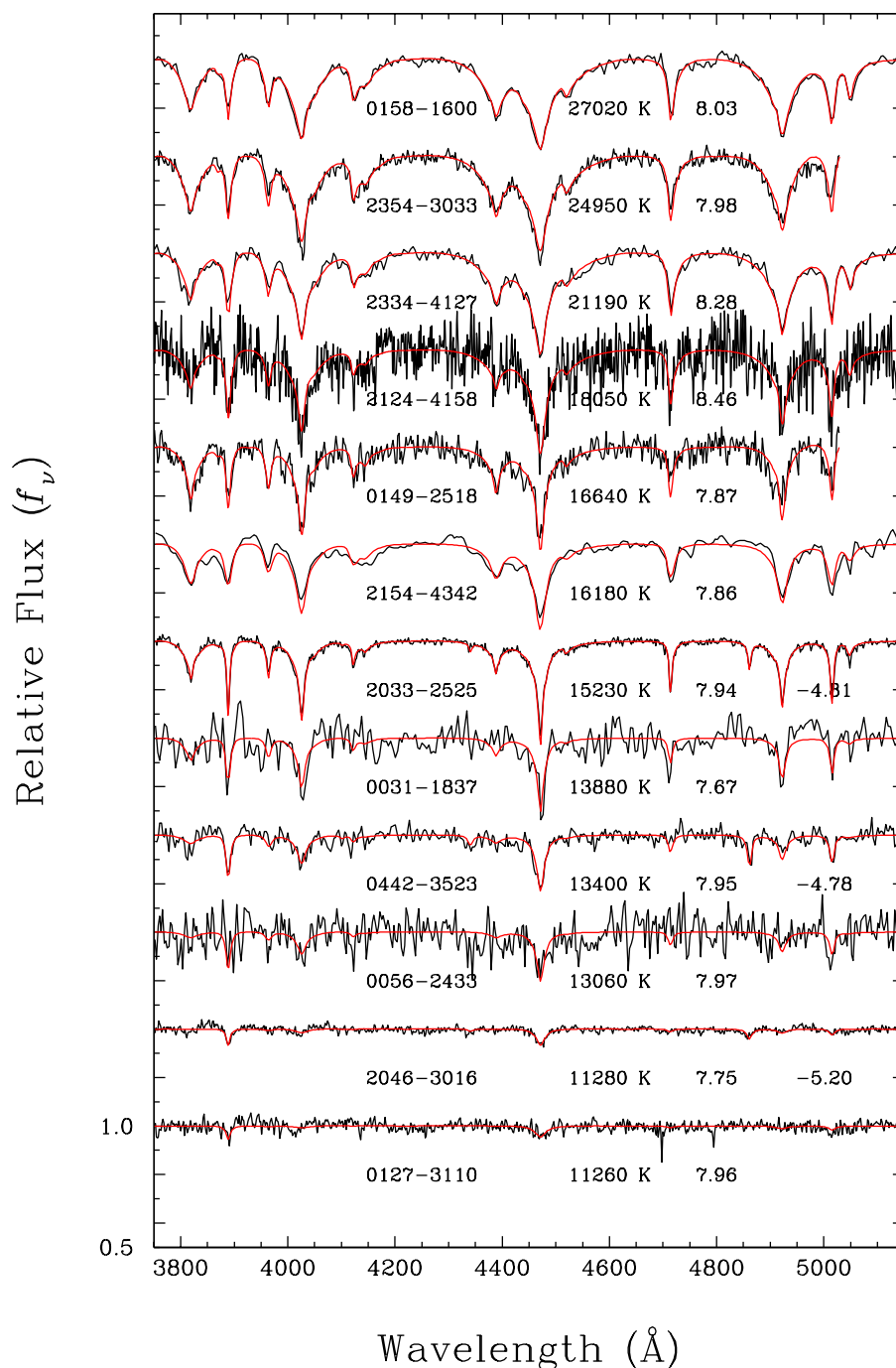


Fig. 9.— Model fits (red) to the normalized spectra (black) for the DB and DBA white dwarfs in our sample, in order of decreasing effective temperature, from top to bottom. The best-fit T_{eff} and $\log g$ values — as well as $\log \text{H/He}$ for DBA stars — are indicated under each spectrum.

this star. Consequently, our atmospheric parameters for the three aforementioned objects should be taken with caution.

For the DC stars in our sample, it is not possible to measure the physical parameters using the spectroscopic technique since these objects are featureless. Here we take advantage of the available *Gaia* observational data and estimate the effective temperature and stellar radius using the photometric technique (Bergeron et al. 1997), where the energy distribution built from the *Gaia* G , G_{BP} , and G_{RP} photometry (EDR3) is fitted with synthetic photometry obtained from model atmospheres. In this case, the fitted parameters are the effective temperature, T_{eff} , and the solid angle, $\pi(R/D)^2$, where R is the radius of the star, and D its distance from Earth obtained from the *Gaia* parallax measurement. Also, interstellar reddening is taken into account since several objects in our sample are sufficiently distant (see Bergeron et al. 2019 for details). The photometric fits are not shown here, and the physical parameters for these DC stars are provided in the next section. As a reminder, we also used this photometric approach to discriminate between the cool and hot spectroscopic solutions for the DA stars.

Finally, the only DQ star in our sample is fitted using a hybrid approach between the spectroscopic and photometric methods. More specifically, we first fit the photometric energy distribution to measure the stellar radius and thus the mass and surface gravity through the mass-radius relation for white dwarfs. Then we force this $\log g$ value and fit the optical spectra with only T_{eff} and C/He — the carbon-to-helium abundance ratio (in number) — as independent parameters. We also assume H/He = 0. Throughout, we rely on the detailed model atmospheres for DQ stars described in Blouin et al. (2019). Our best fit is displayed in Figure 11 with the adopted atmospheric parameters reported in the figure. With an inferred mass of $1.08 M_{\odot}$ (see below), MCT 2137–3651 belongs to this sequence of massive “warm” DQ white dwarfs identified in Figure 12 of Coutu et al. (2019), with the largest carbon abundance ever detected, although this conclusion will require a more detailed analysis than that performed here.

4. Global Properties of the Sample

We summarize in Table 2 the results of our analysis for the 144 white dwarfs in our sample, where we give for each entry the MCT number, the spectral type, the Gaia ID (EDR3), the effective temperature (T_{eff} , rounded off to the nearest 10 K), the surface gravity ($\log g$), the stellar mass (M) — together with uncertainties —, the assumed atmospheric composition, the parallactic distance (D , if available), and the white dwarf cooling time ($\log \tau$ with τ in years). A note added in the last column indicates whether the object

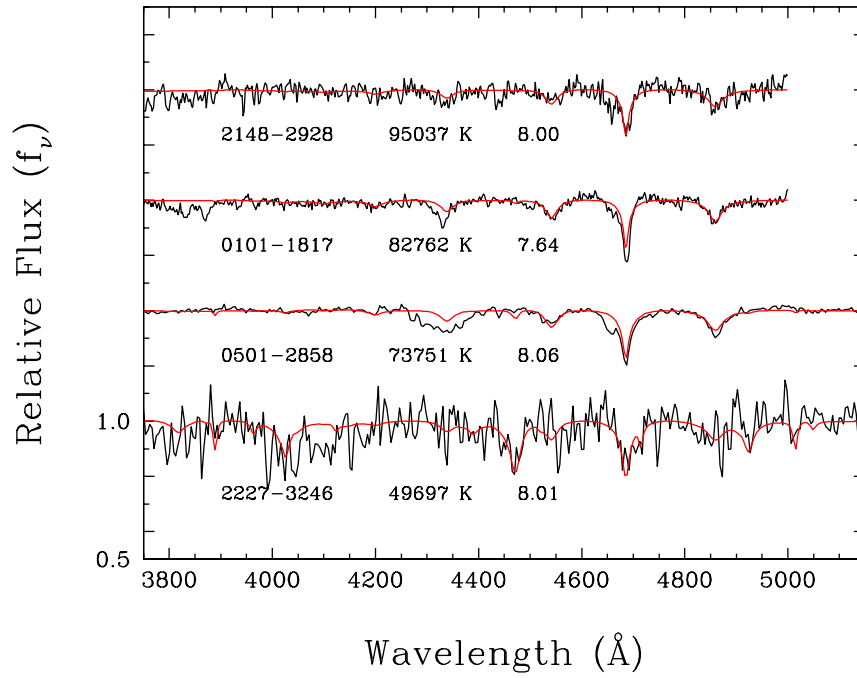


Fig. 10.— Model fits (red) to the normalized spectra (black) for the DO white dwarfs in our sample, in order of decreasing effective temperature, from top to bottom. The best-fit T_{eff} and $\log g$ values are indicated under each spectrum.

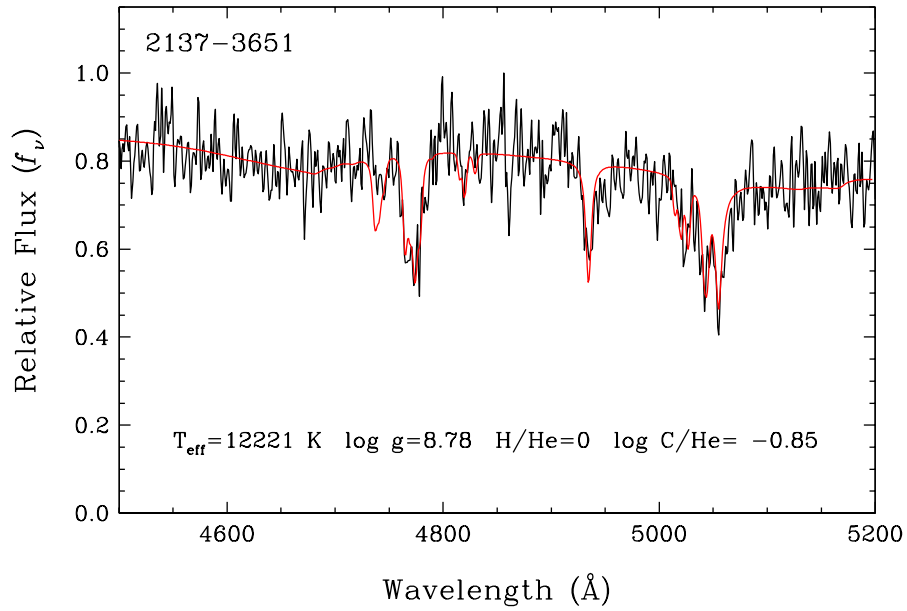


Fig. 11.— Spectroscopic fit to the only DQ white dwarf in our sample. The adopted atmospheric parameters are given in the figure. Note that the $\log g$ value is taken from the photometric fit to the *Gaia* data, and that H/He is assumed to be zero.

has been fitted photometrically instead of spectroscopically, and whether a spectral type is already available in the MWDD. Note that many of these previously known spectral types are taken from the Villanova White Dwarf Catalog of McCook & Sion (1999), where the quoted spectral type actually comes from the MCT survey in a private communication (see, e.g., MCT 0458–3020).

With both fitting techniques, one must rely on mass-radius relations obtained from detailed evolutionary models to infer masses and cooling ages. Here we use the improved cooling sequences and interpolation scheme discussed at length in Bédard et al. (2020). These models — also publicly available on our Web site (see footnote above) — have C/O-core (50/50) compositions, $q(\text{He}) \equiv M_{\text{He}}/M_{\star} = 10^{-2}$, and $q(\text{H}) = 10^{-4}$ or 10^{-10} , which we use for DA and non-DA stars, respectively. Note that some of the cooling times are omitted from Table 2 because they are too small. As discussed by Bédard et al., very short cooling ages ($\log \tau \lesssim 5$) are sensitive to the zero points set by the initial models of the cooling sequences. In such cases, one can simply state an upper limit of $\log \tau < 5$.

As discussed above, the values of T_{eff} and $\log g$ for the DA stars have been determined spectroscopically using model atmospheres calculated within the mixing-length theory, the so-called 1D models. Such 1D models are well-known to yield spurious high- $\log g$ values for white dwarfs below $T_{\text{eff}} \sim 12,000$ K (see the full discussion of this problem in Tremblay et al. 2010). This long-standing high- $\log g$ problem has been solved by Tremblay et al. (2011b), who showed that the use of more sophisticated 3D hydrodynamical model atmospheres yields $\log g$ values that are significantly reduced. Consequently, we applied in Table 2 the 3D corrections of Tremblay et al. (2013) to both T_{eff} and $\log g$ for the DA stars in the appropriate range of temperature where convection is important. Note that in principle, similar 3D corrections should also be applied to DB white dwarfs (Cukanovaite et al. 2021). However, as discussed by Cukanovaite et al., given the uncertainties in the microphysical calculations of DB model atmospheres, these 3D corrections are likely to change, and we simply refrain from applying them to the DB parameters in Table 2 (see also Barnett et al. 2021).

The mass distribution of all white dwarfs in the MCT sample is displayed in Figure 12 as a function of effective temperature. Also shown are theoretical isochrones, labeled in units of Gyr, obtained from our evolutionary models. In this figure, we distinguish white dwarfs with H-dominated (red symbols) and He-dominated (cyan symbols) atmospheres. The masses of all white dwarfs appear evenly distributed around the mean canonical mass of $0.6 M_{\odot}$, also shown in the figure. There are four known ZZ Ceti variables in the MCT sample, indicated in Table 2; given its location in Figure 12, MCT 0142–3026 would represent a good ZZ Ceti candidate.

For the DC white dwarfs in our sample, which have been fitted using the photomet-

ric technique, we assumed a varying value of H/He as a function of T_{eff} , as prescribed in Kilic et al. (2020). Such a non-zero hydrogen abundance is required in order to avoid overestimating the photometric masses, as discussed at length in Bergeron et al. (2019, see their Figures 10 and 11). We note that the inferred photometric masses for these cool DC stars are all below $0.6 M_{\odot}$, but that they also align nicely with the warmer DB white dwarfs analyzed with the spectroscopic technique.

Our white dwarf sample includes the usual high- and low-mass objects usually identified in such surveys. In particular, MCT 2035–4236, MCT 2336–1842, and MCT 2354–1510 have spectroscopic masses well below $0.4 M_{\odot}$, and are thus most likely unresolved double degenerate binaries. We also include in this list of double degenerate candidates (noted in Table 2) two white dwarfs with extremely low photometric masses, and with photometric temperatures that differ significantly from the spectroscopic values: MCT 0028–4729 ($T_{\text{phot}} = 13,148$ K, $M_{\text{phot}} = 0.234 M_{\odot}$) and MCT 0145–7035 ($T_{\text{phot}} = 12,813$ K, $M_{\text{phot}} = 0.289 M_{\odot}$).

The cumulative mass distribution, regardless of temperature, is displayed in Figure 13. The mean mass of our sample, $\langle M \rangle = 0.614 M_{\odot}$, and dispersion, $\sigma_M = 0.131 M_{\odot}$, are entirely consistent with the values reported by Genest-Beaulieu & Bergeron (2019, see their Figure 21) for the DA and DB white dwarfs in the SDSS. Only three white dwarfs with masses in excess of $1.0 M_{\odot}$ can be identified in Figures 12 and 13: MCT 0136–2010, MCT 0308–2305, and MCT 2137–3651 (the only DQ star in our sample). This is typical of UV-excess magnitude-limited surveys, which tend to underestimate the number of massive white dwarfs, due to their intrinsic small radii and low luminosities (Liebert et al. 2005).

5. Concluding Remarks

We presented spectroscopic observations of 144 white dwarfs secured in the course of the MCT survey in the southern hemisphere, including 120 DA, 12 DB, 4 DO, 1 DQ, and 7 DC stars. Our main goal was to provide spectral types for the ongoing effort to confirm spectroscopically all white dwarf candidates in the *Gaia* survey, as well as to make available our spectra to the scientific community through the MWDD. We also included in the MWDD the spectra of MCT 0128–3846, MCT 0130–1937, and MCT 0453–2933, displayed in Figure 6 and already analyzed elsewhere in the literature. Although not discussed here, the spectra of many hot subdwarfs have been secured as part of the MCT survey, and these can be made available upon request.

We would like to dedicate this paper to two of the coauthors, F. Wesemael and G. Fontaine,

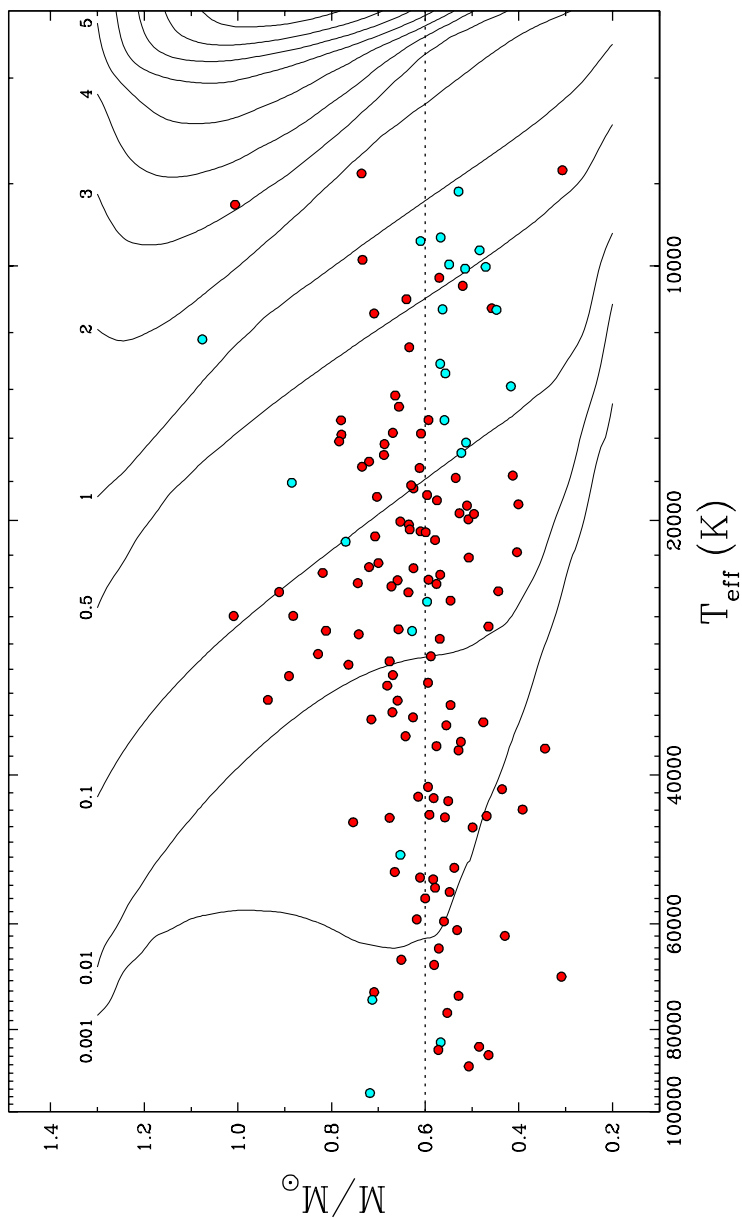


Fig. 12.— Distribution of mass as a function of effective temperature for all the H-atmosphere (red symbols) and He-atmosphere (cyan symbols) white dwarfs in our sample. Also shown as solid lines are the theoretical isochrones from our CO-core evolutionary models, labeled with the white dwarf cooling age in Gyr. The dotted line at $0.6 M_{\odot}$ serves as a reference.

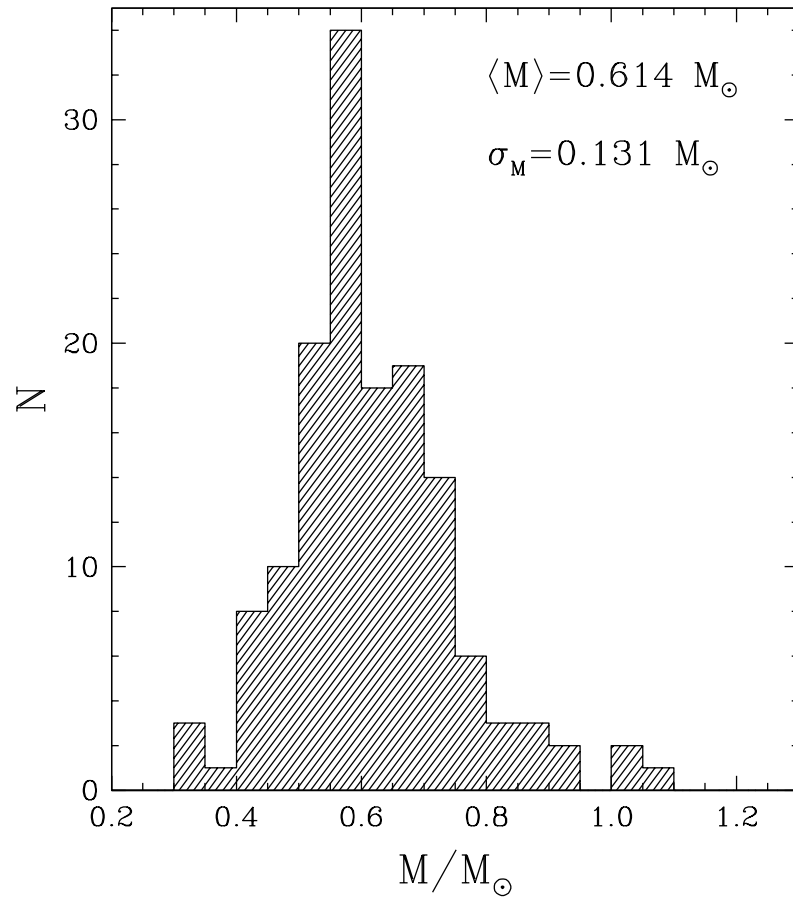


Fig. 13.— Cumulative mass distribution for all white dwarfs in our sample. The mean mass and standard deviation are given in the figure.

who passed away in recent years (2011 and 2019, respectively). Their contribution to the white dwarf field will long be remembered. We are grateful to the CTIO Time Allocation Committee for its unwavering support of this project, and to the CTIO staff for its help and technical support over the years. L. Murphy and A. Beauchamp participated to some of the observing runs at Cerro Tololo and Las Campanas. This work was supported in part by the NSERC Canada, by the Fund FQR-NT (Québec), and by NATO.

Table 1. Photometric and Spectroscopic Data

MCT	RA (B1950.0)	Dec (B1950.0)	B_{pg}	$(U - B)_{pg}$	Date	Telescope	Res (Å)
0000–1838	00 00 37.71	–18 38 39.1	16.29	–0.82	16/10/89	CTIO 4 m	5
0012–1720	00 12 45.41	–17 20 45.0	16.75	–1.02	15/10/89	CTIO 4 m	5
0016–2553	00 16 13.26	–25 53 19.1	16.07	–0.74	09/10/89	CTIO 4 m	3
0024–1211	00 24 00.70	–12 11 23.2	16.26	–0.66	16/10/89	CTIO 4 m	5
0027–6341	00 27 39.71	–63 41 31.4	15.29	–1.03	13/11/92	CTIO 1.5 m	6
0028–4729	00 28 22.78	–47 29 10.0	15.34	–0.69	02/10/88	CTIO 1.5 m	6
0031–1837	00 31 10.35	–18 37 01.5	15.68	–0.88	08/10/89	CTIO 1.5 m	6
0031–3107	00 31 56.97	–31 07 56.7	16.43	–0.96	06/12/95	CTIO 1.5 m	5
0032–1313	00 32 55.84	–13 13 36.1	16.82	–0.93	08/12/95	CTIO 1.5 m	5
0032–1735	00 32 46.26	–17 35 21.6	15.38	–0.75	06/10/89	CTIO 1.5 m	6
0032–3146	00 32 22.17	–31 46 26.5	15.62	–0.91	08/10/89	CTIO 1.5 m	6
0033–3440	00 33 47.03	–34 40 01.8	16.42	–0.69	06/12/95	CTIO 1.5 m	5
0049–2658	00 49 08.82	–26 58 13.9	16.42	–0.91	07/12/95	CTIO 1.5 m	5
0050–3316	00 50 53.50	–33 16 12.3	13.30	–1.20	12/11/92	CTIO 1.5 m	6
0052–1442	00 52 26.04	–14 42 20.3	14.95	–1.03	04/09/85	CTIO 1.5 m	13
0056–2433	00 56 43.45	–24 33 40.7	16.36	–0.73	07/12/95	CTIO 1.5 m	5
0101–1817	01 01 47.32	–18 17 45.3	15.26	–1.00	04/09/85	CTIO 1.5 m	13
0102–1835	01 02 25.55	–18 35 48.7	16.40	–0.61	14/09/94	CTIO 4 m	3
0105–1634	01 05 41.73	–16 34 39.4	16.44	–0.73	14/09/94	CTIO 4 m	3
0106–3550	01 06 01.02	–35 50 39.1	14.75	–1.08	04/09/85	CTIO 1.5 m	13
0110–1355	01 10 41.53	–13 55 19.6	15.68	–0.96	07/10/89	CTIO 1.5 m	6
0110–1617	01 10 46.37	–16 17 36.7	16.37	–0.60	07/12/95	CTIO 1.5 m	5
0111–3806	01 11 45.83	–38 06 33.5	15.48	–1.09	08/10/89	CTIO 1.5 m	6
0112–1931	01 12 39.31	–19 31 07.0	16.20	–0.73	15/10/89	CTIO 4 m	5
0118–1638	01 18 31.78	–16 38 28.9	15.90	–0.64	09/10/89	CTIO 1.5 m	6
0124–2546	01 24 33.91	–25 46 20.5	15.66	–0.60	09/10/89	CTIO 1.5 m	6
0127–3110	01 27 37.56	–31 10 37.6	15.61	–0.81	08/10/89	CTIO 1.5 m	6
0129–2035	01 29 14.90	–20 35 22.8	14.64	–0.62	01/10/88	CTIO 1.5 m	6
0130–6846	01 30 30.27	–68 46 35.2	14.53	–0.98	16/11/86	CTIO 1.5 m	7
0131–1622	01 31 58.00	–16 22 26.2	13.96	–1.38	31/08/85	CTIO 1.5 m	13
0133–3846	01 33 03.94	–38 46 52.0	16.32	–0.69	14/10/89	CTIO 4 m	5
0134–4042	01 34 37.67	–40 42 49.4	16.46	–0.86	14/09/94	CTIO 4 m	3
0136–2010	01 36 08.17	–20 10 01.5	16.49	–0.64	01/07/94	La Palma 2.5 m	6
0137–2908	01 37 58.49	–29 08 01.8	16.04	–0.65	09/10/89	CTIO 4 m	3
0138–2336	01 38 06.61	–23 36 29.5	16.10	–0.89	09/10/89	CTIO 4 m	3
0138–4014	01 38 00.87	–40 14 34.9	16.10	–0.67	15/09/94	CTIO 4 m	3
0140–3914	01 40 40.47	–39 14 12.7	14.43	–0.97	14/11/86	CTIO 1.5 m	7
0142–3026	01 42 19.45	–30 26 24.5	16.46	–0.65	08/12/95	CTIO 1.5 m	5
0145–2211	01 45 00.17	–22 11 46.6	15.30	–0.66	29/09/88	CTIO 1.5 m	6
0145–7035	01 45 01.40	–70 35 15.6	15.31	–0.82	02/10/88	CTIO 1.5 m	6
0146–2500	01 46 19.70	–25 00 37.4	16.37	–0.69	08/12/95	CTIO 1.5 m	5
0149–2518	01 49 40.50	–25 18 00.4	15.91	–0.72	14/10/89	CTIO 4 m	5
0154–2405	01 54 52.62	–24 05 59.0	16.36	–1.11	24/09/88	CTIO 4.0 m	7
0158–1600	01 58 32.36	–16 00 38.9	14.38	–0.99	29/09/88	CTIO 1.5 m	6
0158–2242	01 58 33.57	–22 42 03.5	16.10	–1.01	15/10/89	CTIO 4 m	5
0200–1243	02 00 38.15	–12 43 21.8	14.75	–0.89	06/10/89	CTIO 1.5 m	6

Table 1—Continued

MCT	RA (B1950.0)	Dec (B1950.0)	B_{pg}	$(U - B)_{pg}$	Date	Telescope	Res (Å)
0203–1807	02 03 01.31	–18 07 43.8	15.48	–0.69	06/10/89	CTIO 1.5 m	6
0205–3025	02 05 27.35	–30 25 09.8	15.67	–0.60	01/10/88	CTIO 1.5 m	6
0205–3635	02 05 17.64	–36 35 03.1	16.10	–1.00	15/10/89	CTIO 4 m	5
0208–1520	02 08 18.90	–15 20 40.4	15.56	–0.67	07/10/89	CTIO 1.5 m	6
0208–2621	02 08 42.66	–26 21 06.7	16.15	–0.83	15/10/89	CTIO 4 m	5
0210–3929	02 10 39.93	–39 29 54.4	16.48	–0.64	08/12/95	CTIO 1.5 m	5
0212–2308	02 12 03.16	–23 08 46.5	16.08	–0.73	15/10/89	CTIO 4 m	5
0219–4049	02 19 18.92	–40 49 10.7	16.21	–0.66	05/12/95	CTIO 1.5 m	5
0221–2642	02 21 15.04	–26 42 54.0	15.62	–1.21	11/09/94	CTIO 1.5 m	6
0222–2630	02 22 21.60	–26 30 24.1	15.55	–0.77	11/09/94	CTIO 1.5 m	6
0226–3255	02 26 19.39	–32 55 50.7	13.90	–1.03	13/11/86	CTIO 1.5 m	7
0235–1234	02 35 01.60	–12 34 31.3	14.78	–1.11	13/11/92	CTIO 1.5 m	6
0252–3501	02 52 35.43	–35 01 58.3	15.80	–0.63	17/10/89	CTIO 4 m	5
0257–3339	02 57 01.69	–33 39 31.5	16.03	–1.02	04/12/95	CTIO 1.5 m	5
0300–2313	03 00 23.21	–23 13 35.5	15.66	–1.02	12/09/94	CTIO 1.5 m	6
0308–2305	03 08 54.29	–23 05 21.3	15.19	–1.03	12/09/94	CTIO 1.5 m	6
0309–2105	03 09 43.30	–21 05 22.5	15.76	–0.81	06/12/95	CTIO 1.5 m	5
0309–2730	03 09 25.05	–27 30 41.1	16.21	–0.80	24/09/88	CTIO 4.0 m	7
0315–3313	03 15 25.40	–33 13 57.8	16.53	–0.97	23/09/88	CTIO 4.0 m	7
0320–5355	03 20 51.40	–53 55 55.3	14.99	–1.19	25/09/93	CTIO 1.5 m	6
0333–3500	03 33 38.11	–35 00 07.5	15.51	–0.77	13/11/86	CTIO 1.5 m	7
0335–4205	03 35 29.96	–42 05 06.7	15.98	–1.41	06/12/95	CTIO 1.5 m	5
0341–6719	03 41 59.62	–67 19 03.9	15.78	–0.82	07/12/95	CTIO 1.5 m	5
0400–4045	04 00 57.85	–40 45 59.8	15.75	–0.67	06/12/95	CTIO 1.5 m	5
0413–4029	04 13 57.09	–40 29 56.3	15.98	–0.96	07/12/95	CTIO 1.5 m	5
0420–7310	04 20 23.65	–73 10 45.0	15.49	–0.72	30/09/88	CTIO 1.5 m	6
0442–3523	04 42 38.30	–35 23 14.0	15.72	–0.68	07/12/95	CTIO 1.5 m	5
0455–2812	04 55 13.97	–28 12 25.3	13.91	–1.28	00/00/00	Steward 2.3 m	6
0458–3020	04 58 46.54	–30 20 56.1	16.30	–0.99	17/10/89	CTIO 4 m	5
0501–2858	05 01 57.61	–28 58 39.1	14.09	–1.36	13/11/86	CTIO 1.5 m	7
1950–4314	19 50 18.33	–43 14 59.7	14.89	–1.41	31/08/85	CTIO 1.5 m	13
1958–5008	19 58 04.38	–50 08 23.2	15.17	–1.09	26/07/89	MWLCO 2.5 m	3
2000–5611	20 00 18.67	–56 11 15.4	14.97	–1.27	27/07/89	MWLCO 2.5 m	3
2001–5349	20 01 03.48	–53 49 22.9	16.22	–0.67	14/10/89	CTIO 4 m	5
2002–5405	20 02 33.27	–54 05 42.2	16.14	–1.20	14/10/89	CTIO 4 m	5
2004–3021	20 04 25.00	–30 21 08.4	16.03	–0.69	08/10/89	CTIO 1.5 m	6
2017–3726	20 17 00.55	–37 26 09.8	16.43	–0.79	08/08/88	MWLCO 2.5 m	3
2019–3438	20 19 45.79	–34 38 11.7	16.46	–1.04	08/08/88	MWLCO 2.5 m	3
2020–4234	20 20 35.96	–42 34 08.8	14.79	–0.81	10/08/88	MWLCO 2.5 m	3
2031–2745	20 31 53.30	–27 45 10.6	14.73	–1.16	11/09/94	CTIO 1.5 m	6
2033–2525	20 33 47.24	–25 25 06.5	15.12	–1.02	11/09/94	CTIO 1.5 m	6
2035–3337	20 35 30.02	–33 37 09.6	14.57	–1.02	10/08/88	MWLCO 2.5 m	3
2035–4236	20 35 48.09	–42 36 46.9	16.86	–1.30	09/08/88	MWLCO 2.5 m	3
2040–3914	20 40 34.06	–39 14 05.4	14.29	–0.64	10/08/88	MWLCO 2.5 m	3
2046–3016	20 46 28.09	–30 16 10.9	15.74	–0.88	26/07/89	MWLCO 2.5 m	3
2100–3821	21 00 03.78	–38 21 33.6	15.97	–0.84	09/08/88	MWLCO 2.5 m	3

Table 1—Continued

MCT	RA (B1950.0)	Dec (B1950.0)	B_{pg}	$(U - B)_{pg}$	Date	Telescope	Res (Å)
2100–3840	21 00 11.66	–38 40 09.3	16.23	–0.96	09/08/88	MWLCO 2.5 m	3
2101–3627	21 01 38.84	–36 27 22.5	16.10	–0.91	10/08/88	MWLCO 2.5 m	3
2103–3947	21 03 19.75	–39 47 55.9	15.42	–0.48	28/09/88	CTIO 1.5 m	6
2107–2653	21 07 18.35	–26 53 39.2	16.11	–1.10	14/10/89	CTIO 4 m	5
2108–4310	21 08 21.45	–43 10 27.3	16.03	–0.67	15/10/89	CTIO 4 m	5
2109–2934	21 09 41.30	–29 34 36.2	15.44	–0.65	26/07/89	MWLCO 2.5 m	3
2113–3705	21 13 41.55	–37 05 05.8	16.38	–0.67	11/08/88	MWLCO 2.5 m	3
2114–3737	21 14 17.52	–37 37 07.2	15.64	–0.76	08/08/88	MWLCO 2.5 m	3
2122–4643	21 22 11.83	–46 43 33.9	15.99	–0.67	15/10/89	CTIO 4 m	5
2124–4158	21 24 25.23	–41 58 22.1	15.89	–0.89	13/08/88	MWLCO 2.5 m	3
2133–3637	21 33 35.91	–36 37 26.8	15.74	–0.80	08/08/88	MWLCO 2.5 m	3
2137–3651	21 37 21.65	–36 51 33.4	15.96	–0.85	10/08/88	MWLCO 2.5 m	3
2137–3756	21 37 14.63	–37 56 21.6	16.03	–0.67	11/08/88	MWLCO 2.5 m	3
2146–4320	21 46 31.05	–43 20 12.8	15.85	–1.21	10/08/88	MWLCO 2.5 m	3
2148–2910	21 48 45.90	–29 10 51.7	15.99	–0.64	14/10/89	CTIO 4 m	5
2148–2928	21 48 24.79	–29 28 43.4	16.30	–0.98	15/10/89	CTIO 4 m	5
2151–3043	21 51 58.72	–30 43 31.9	14.82	–0.78	26/07/89	MWLCO 2.5 m	3
2153–4156	21 53 30.56	–41 56 31.2	15.67	–1.05	11/08/88	MWLCO 2.5 m	3
2154–4342	21 54 54.79	–43 42 12.9	14.82	–0.83	02/09/85	CTIO 1.5 m	13
2159–4129	21 59 25.55	–41 29 00.6	15.54	–1.09	03/09/85	CTIO 1.5 m	13
2214–3740	22 14 49.76	–37 40 42.3	15.93	–0.99	01/10/88	CTIO 1.5 m	6
2227–3246	22 27 58.77	–32 46 56.3	15.84	–0.97	01/10/88	CTIO 1.5 m	6
2231–2935	22 31 39.20	–29 35 15.1	15.73	–0.98	26/07/89	MWLCO 2.5 m	3
2233–3529	22 33 58.95	–35 29 40.9	15.28	–0.89	10/09/94	CTIO 1.5 m	6
2241–4031	22 41 28.80	–40 31 21.7	15.99	–0.79	14/09/94	CTIO 4 m	3
2251–6326	22 51 58.89	–63 26 30.0	14.28	–0.96	13/08/88	MWLCO 2.5 m	3
2252–4042	22 52 51.57	–40 42 21.0	15.70	–1.09	12/09/94	CTIO 1.5 m	6
2259–2646	22 59 20.34	–26 46 56.5	15.18	–0.76	13/08/88	MWLCO 2.5 m	3
2259–3212	22 59 28.62	–32 12 07.4	15.98	–1.07	23/09/88	CTIO 4.0 m	7
2306–2726	23 06 10.54	–27 26 41.9	15.88	–0.56	30/09/88	CTIO 1.5 m	6
2311–2605	23 11 12.69	–26 05 04.5	16.05	–1.23	12/08/88	MWLCO 2.5 m	3
2313–3303	23 13 20.65	–33 03 02.2	15.74	–1.09	23/09/88	CTIO 4.0 m	7
2318–2236	23 18 47.63	–22 36 40.9	16.05	–0.88	23/09/88	CTIO 4.0 m	7
2322–1808	23 22 41.04	–18 08 27.1	15.31	–0.96	11/08/88	MWLCO 2.5 m	3
2326–2226	23 26 01.11	–22 26 48.0	15.85	–0.48	30/09/88	CTIO 1.5 m	6
2329–3317	23 29 31.79	–33 17 37.2	16.24	–0.78	12/08/88	MWLCO 2.5 m	3
2330–2113	23 30 22.59	–21 13 44.1	16.25	–0.74	14/10/89	CTIO 4 m	5
2331–4731	23 31 19.78	–47 31 00.1	13.59	–1.18	18/08/87	CTIO 1.5 m	6
2333–1634	23 33 00.57	–16 34 16.3	13.80	–0.91	28/09/88	CTIO 1.5 m	6
2334–4127	23 34 58.73	–41 27 07.7	15.28	–1.15	09/09/94	CTIO 1.5 m	6
2336–1842	23 36 16.75	–18 42 46.9	15.84	–0.64	23/09/88	CTIO 4.0 m	7
2336–1955	23 36 51.69	–19 55 23.4	16.30	–0.74	16/10/89	CTIO 4 m	5
2343–1740	23 43 50.50	–17 40 54.1	16.12	–1.04	01/07/94	La Palma 2.5 m	6
2345–3940	23 45 49.42	–39 40 27.2	16.06	–1.01	14/09/94	CTIO 4 m	3
2347–1916	23 47 28.08	–19 16 02.0	15.38	–0.90	03/09/85	CTIO 1.5 m	13
2349–2819	23 49 47.87	–28 19 53.9	15.54	–0.86	06/10/89	CTIO 1.5 m	6

Table 1—Continued

MCT	RA (B1950.0)	Dec (B1950.0)	B_{pg}	$(U - B)_{\text{pg}}$	Date	Telescope	Res (\AA)
2349–3627	23 49 32.40	–36 27 22.9	16.41	–1.18	14/09/94	CTIO 4 m	3
2350–2448	23 50 28.94	–24 48 43.4	15.21	–1.02	29/09/88	CTIO 1.5 m	6
2352–1249	23 52 39.63	–12 49 34.4	16.49	–0.71	15/09/94	CTIO 4 m	3
2354–1510	23 54 59.41	–15 10 49.0	15.02	–0.98	01/10/88	CTIO 1.5 m	6
2354–3033	23 54 02.78	–30 33 02.1	16.26	–0.78	16/10/89	CTIO 4 m	5
2359–3228	23 59 58.46	–32 28 26.1	15.87	–0.64	24/09/88	CTIO 4.0 m	7

Table 2. Atmospheric Parameters of MCT White Dwarfs

MCT	Type	Gaia ID (EDR3)	T_{eff} (K)	$\log g$	M/M_{\odot}	Comp	$D(\text{pc})$	$\log \tau$	Notes
0000–1838	DA	2414099622710507904	15,220 (279)	7.96 (0.05)	0.59 (0.03)	H	99	8.26	1
0012–1720	DA	2368091860020553472	54,980 (1809)	7.64 (0.12)	0.55 (0.04)	H	360	6.09	
0016–2553	DA	2323704339384503040	10,950 (176)	8.06 (0.06)	0.64 (0.04)	H	61	8.74	1, 2
0024–1211	DA	2423844216310164864	15,790 (285)	7.99 (0.05)	0.61 (0.03)	H	104	8.23	1
0027–6341	DA	4900807999725863296	59,560 (1615)	7.64 (0.10)	0.56 (0.03)	H	197	5.99	1
0028–4729	DA	4978793541987799040	17,820 (357)	7.84 (0.06)	0.54 (0.03)	H	96	7.89	3
0031–1837	DB	2363965672055370112	13,880 (716)	7.67 (0.43)	0.42 (0.19)	He	113	8.19	1
0031–3107	DA	2317553529604662016	42,420 (1474)	7.88 (0.15)	0.61 (0.07)	H	439	6.50	1
0032–1313	DA+dM	2375355375568178304	72,230 (6089)	7.96 (0.30)	0.71 (0.13)	H	263	5.84	
0032–1735	DA	2364319061964016512	9840 (180)	8.22 (0.12)	0.73 (0.07)	H	33	8.95	1
0032–3146	DA	2317319612801004416	43,930 (994)	7.26 (0.09)	0.39 (0.03)	H	431	—	1
0033–3440	DA	5005361213245945856	15,230 (515)	8.27 (0.07)	0.78 (0.05)	H	87	8.48	1
0049–2658	DA	2342910436701710080	34,380 (837)	8.11 (0.14)	0.71 (0.08)	H	277	6.77	1
0050–3316	DA	5006486048001153792	35,980 (575)	7.97 (0.06)	0.64 (0.03)	H	59	6.70	1
0052–1442	DA	2372473658671416960	25,940 (485)	8.41 (0.07)	0.88 (0.04)	H	73	7.82	1
0056–2433	DB	2345088259997529856	13,060 (861)	7.97 (0.56)	0.57 (0.30)	He	102	8.47	
0101–1817	DOZ	2358027755213297408	82,760 (4624)	7.64 (0.20)	0.57 (0.07)	He	400	5.45	1
0102–1835	DA	2357946464368276224	23,780 (381)	7.89 (0.05)	0.58 (0.03)	H	212	7.33	1
0105–1634	DA	2359382697136585728	28,950 (436)	7.89 (0.05)	0.59 (0.03)	H	260	7.00	1
0106–3550	DA	5014009353235167744	30,470 (501)	8.04 (0.07)	0.67 (0.04)	H	93	6.95	1
0110–1355	DA	2456122476087944960	26,900 (800)	8.03 (0.12)	0.66 (0.07)	H	121	7.18	1
0110–1617	DA	2358739727648116608	37,400 (1324)	7.72 (0.17)	0.53 (0.07)	H	345	6.63	1
0111–3806	DA	4988781711771040128	83,790 (2744)	7.12 (0.09)	0.48 (0.02)	H	488	—	1
0112–1931	DA	2354521726165844096	36,970 (899)	7.83 (0.11)	0.58 (0.05)	H	307	6.67	1
0118–1638	DA	2454507602744210432	14,680 (510)	8.07 (0.08)	0.66 (0.05)	H	77	8.39	1
0124–2546	DA	5037128131397095168	23,510 (541)	7.93 (0.07)	0.59 (0.04)	H	162	7.38	1
0127–3110	DB	5016897564123557248	11,260 (479)	7.96 (0.40)	0.56 (0.22)	He	55	8.66	1
0129–2035	DA	5043926824108837376	20,230 (424)	8.02 (0.06)	0.64 (0.04)	H	84	7.82	1
0130–6846	DA	4691571967756922368	34,650 (625)	7.60 (0.09)	0.48 (0.03)	H	210	6.64	1
0131–1622	DA+dM	2451047370931938176	52,870 (1219)	7.83 (0.08)	0.61 (0.04)	H	94	6.24	1
0133–3846	DA	5008992762714188800	16,740 (286)	8.12 (0.05)	0.69 (0.03)	H	117	8.25	1
0134–4042	DA+dM	4960508526175740928	34,930 (560)	7.79 (0.07)	0.56 (0.03)	H	264	6.74	1
0136–2010	DA	5139880551029408768	8470 (123)	8.64 (0.06)	1.01 (0.03)	H	24	9.49	1
0137–2908	DA	5023333658515040128	24,260 (532)	7.60 (0.07)	0.44 (0.03)	H	158	7.17	1
0138–2336	DA	5039292451317431168	36,540 (782)	7.71 (0.10)	0.52 (0.04)	H	482	6.65	1
0138–4014	DA	4960499042889705344	23,540 (530)	8.05 (0.07)	0.66 (0.04)	H	138	7.50	1
0140–3914	DA	4962193390308361728	23,720 (535)	8.19 (0.07)	0.74 (0.04)	H	58	7.70	1
0142–3026	DA	5022387185162024960	11,220 (262)	7.73 (0.12)	0.46 (0.06)	H	84	8.51	1
0145–2211	DA	5135466183642594304	11,390 (263)	8.17 (0.10)	0.71 (0.06)	H	46	8.76	1, 2

Table 2—Continued

MCT	Type	Gaia ID (EDR3)	T_{eff} (K)	$\log g$	M/M_{\odot}	Comp	$D(\text{pc})$	$\log \tau$	Notes
0145–7035	DA	4687960621811310976	19,210 (426)	7.79 (0.07)	0.51 (0.03)	H	122	7.68	3
0146–2500	DA	5038054122050564864	21,810 (873)	7.51 (0.12)	0.40 (0.04)	H	301	7.29	1
0149–2518	DB	5026000176075186560	16,640 (544)	7.87 (0.23)	0.52 (0.12)	He	147	8.04	1
0154–2405	DA	5122240020833180416	76,420 (3538)	7.46 (0.16)	0.55 (0.05)	H	545	5.27	1
0158–1600	DB	5147930591051748480	27,020 (1788)	8.03 (0.08)	0.63 (0.04)	He	68	7.19	
0158–2242	DA	5134814168951616000	72,940 (3210)	7.43 (0.15)	0.53 (0.05)	H	594	—	
0200–1243	DC	5149836834977282048	9350 (39)	8.05 (0.01)	0.61 (0.00)	$\log \text{H}/\text{He}=-4.4$	24	8.92	4
0203–1807	DC	5138313850039513472	10,030 (89)	7.80 (0.02)	0.47 (0.01)	$\log \text{H}/\text{He}=-4.6$	52	8.70	4
0205–3025	DA	5020146620982523008	18,330 (576)	8.01 (0.10)	0.62 (0.06)	H	87	8.00	
0205–3635	DA	4968128554074903808	67,060 (1887)	7.65 (0.10)	0.58 (0.03)	H	382	5.87	1
0208–1520	DA+dM	5148232991109667328	20,890 (390)	8.14 (0.06)	0.71 (0.03)	H	96	7.90	1
0208–2621	DA	5118133276183878400	33,720 (544)	8.03 (0.07)	0.67 (0.04)	H	250	6.79	1
0210–3929	DC	4964236282912470400	8170 (63)	7.92 (0.01)	0.53 (0.01)	$\log \text{H}/\text{He}=-3.8$	54	8.99	4
0212–2308	DA	5123291871208145792	27,270 (468)	8.18 (0.06)	0.74 (0.04)	H	184	7.31	
0219–4049	DA	4951125156507440384	15,760 (295)	8.09 (0.05)	0.67 (0.03)	H	100	8.31	
0221–2642	DA	5118624311204821504	33,060 (567)	7.78 (0.08)	0.55 (0.04)	H	178	6.80	
0222–2630	DA	5118634309888681600	24,320 (448)	8.00 (0.06)	0.64 (0.03)	H	108	7.37	
0226–3255	DA	5063539946887524864	22,710 (551)	8.15 (0.08)	0.72 (0.05)	H	44	7.74	1
0235–1234	DA	5170668766392712448	32,600 (520)	8.48 (0.07)	0.94 (0.04)	H	70	7.39	1
0252–3501	DA	5049628376014475648	17,710 (283)	7.57 (0.05)	0.41 (0.02)	H	130	7.69	1
0257–3339	DA	5051294582807658240	44,570 (1616)	7.82 (0.15)	0.59 (0.07)	H	272	6.44	
0300–2313	DA	5078074837769743744	24,300 (457)	8.46 (0.06)	0.91 (0.04)	H	79	8.00	
0308–2305	DA	5075443981321647744	25,940 (450)	8.62 (0.06)	1.01 (0.04)	H	55	8.06	
0309–2105	DC	5102795329494950784	9970 (94)	7.95 (0.02)	0.55 (0.01)	$\log \text{H}/\text{He}=-4.6$	46	8.79	4
0309–2730	DA+dM	5061294228745514752	61,970 (2533)	7.21 (0.14)	0.43 (0.04)	H	269	—	1
0315–3313	DA	5054287144220982144	46,130 (1314)	7.57 (0.11)	0.50 (0.04)	H	486	6.17	
0320–5355	DA	4734298439852277376	32,660 (571)	8.01 (0.09)	0.66 (0.05)	H	118	6.83	
0333–3500	DA	4861136658123791488	34,180 (518)	7.95 (0.06)	0.63 (0.03)	H	237	6.77	1
0335–4205	DA	4849023441599834112	44,880 (1697)	7.74 (0.16)	0.56 (0.06)	H	295	6.42	
0341–6719	DA	4667932055438729728	15,840 (503)	8.27 (0.08)	0.78 (0.05)	H	63	8.43	
0400–4045	DA	4842472688760384384	10,330 (160)	7.95 (0.07)	0.57 (0.04)	H	45	8.73	
0413–4029	DA	4841120770494891520	53,110 (2129)	7.75 (0.15)	0.58 (0.06)	H	287	6.21	
0420–7310	DA	4653404070862114176	18,760 (428)	8.14 (0.07)	0.70 (0.04)	H	84	8.09	
0442–3523	DBA	4867104257483687040	13,400 (400)	7.95 (0.19)	0.56 (0.11)	$\log \text{H}/\text{He}=-4.8$	59	8.43	
0455–2812	DA	4880286371109059712	59,240 (1454)	7.81 (0.09)	0.62 (0.03)	H	125	6.09	1
0458–3020	DA	4876440794831381760	84,500 (4212)	7.46 (0.16)	0.57 (0.05)	H	681	5.03	1
0501–2858	DOZ	4876967941937370368	73,750 (3527)	8.06 (0.20)	0.71 (0.10)	He	138	5.89	1

Table 2—Continued

MCT	Type	Gaia ID (EDR3)	T_{eff} (K)	$\log g$	M/M_{\odot}	Comp	$D(\text{pc})$	$\log \tau$	Notes
1950–4314	DA	6685284241684914688	41,310 (1160)	7.84 (0.12)	0.59 (0.05)	H	142	6.53	1
1958–5008	DA	6667323341287601024	52,070 (1776)	7.95 (0.13)	0.67 (0.06)	H	149	6.25	
2000–5611	DA	6448025712768292992	42,940 (1278)	7.74 (0.12)	0.55 (0.05)	H	182	6.47	1
2001–5349	DA	6473219235012100096	17,340 (302)	7.99 (0.05)	0.61 (0.03)	H	108	8.08	
2002–5405	DA	6473244283259625088	18,180 (298)	8.02 (0.05)	0.63 (0.03)	H	101	8.02	
2004–3021	DA	6749528431218859392	17,040 (609)	8.17 (0.11)	0.72 (0.07)	H	86	8.26	
2017–3726	DA	6693472717093585664	19,940 (650)	7.78 (0.10)	0.51 (0.05)	H	178	7.60	
2019–3438	DA	6696596356613398144	27,010 (599)	8.29 (0.09)	0.81 (0.05)	H	146	7.54	
2020–4234	DA	6679362959252072832	29,620 (515)	8.21 (0.07)	0.76 (0.04)	H	98	7.13	1
2031–2745	DA	6799465466213872256	55,960 (1080)	7.78 (0.07)	0.60 (0.03)	H	183	6.16	
2033–2525	DBA	6800380775284148864	15,230 (356)	7.94 (0.07)	0.56 (0.04)	$\log \text{H}/\text{He}=-4.8$	61	8.25	
2035–3337	DA	6791907526363085952	19,650 (411)	7.75 (0.07)	0.50 (0.03)	H	53	7.61	1
2035–4236	DA	6676510104534576512	69,230 (6699)	6.52 (0.27)	0.31 (0.06)	H	700	—	3
2040–3914	DA	6681773947733560192	10,560 (165)	7.85 (0.07)	0.52 (0.04)	H	23	8.66	1, 2
2046–3016	DBA	6794613321399870080	11,280 (314)	7.75 (0.18)	0.45 (0.09)	$\log \text{H}/\text{He}=-5.2$	49	8.53	
2100–3821	DA	6774392546650858624	16,250 (362)	8.12 (0.07)	0.69 (0.04)	H	78	8.29	
2100–3840	DA	6774367017365076608	23,930 (656)	8.07 (0.09)	0.67 (0.05)	H	194	7.49	
2101–3627	DA+dM:	6776891083744902784	44,720 (1237)	7.49 (0.11)	0.47 (0.04)	H	349	5.91	
2103–3947	DA	6774018369099513216	7780 (149)	8.23 (0.17)	0.74 (0.11)	H	25	9.23	
2107–2653	DA	6802767849386125440	88,370 (4225)	7.16 (0.14)	0.51 (0.03)	H	577	—	
2108–4310	DA+dM	6580207798067984000	23,080 (466)	8.31 (0.07)	0.82 (0.04)	H	132	7.92	
2109–2934	DC	6788656957673130112	9260 (40)	7.98 (0.01)	0.57 (0.00)	$\log \text{H}/\text{He}=-4.4$	32	8.89	4
2113–3705	DC	6776236530729179136	9590 (95)	7.83 (0.02)	0.48 (0.01)	$\log \text{H}/\text{He}=-4.4$	71	8.76	4
2114–3737	DA	6583681533257898752	23,190 (577)	7.88 (0.08)	0.57 (0.04)	H	119	7.38	1
2122–4643	DA	6575491133702739584	16,130 (276)	8.28 (0.05)	0.78 (0.03)	H	85	8.42	
2124–4158	DB	6578965762246071808	18,050 (741)	8.46 (0.23)	0.89 (0.15)	He	114	8.42	
2133–3637	DA	6589423148617705856	24,880 (571)	7.83 (0.08)	0.55 (0.04)	H	118	7.22	1
2137–3651	DQ	6589369272547881856	12,220 (120)	8.78 (0.01)	1.08 (0.01)	$\log \text{C}/\text{He}=-0.8$	39	9.16	
2137–3756	DA	6585878288771383296	20,500 (686)	8.01 (0.10)	0.63 (0.06)	H	145	7.78	
2146–4320	DA	6565941703417200128	64,130 (2474)	7.64 (0.14)	0.57 (0.04)	H	343	5.92	1
2148–2910	DA	6617454235493798272	12,480 (232)	8.05 (0.06)	0.63 (0.04)	H	74	8.58	1, 2
2148–2928	DOZ	6617395854003241856	95,040 (13197)	8.00 (0.35)	0.72 (0.14)	He	696	5.56	
2151–3043	DA	6616313457820826496	28,770 (558)	8.32 (0.08)	0.83 (0.05)	H	69	7.41	
2153–4156	DA	6572442909513784576	42,590 (2031)	7.81 (0.21)	0.58 (0.09)	H	209	6.49	1
2154–4342	DB	6570892323240774144	16,180 (513)	7.86 (0.23)	0.51 (0.12)	He	50	8.08	
2159–4129	DA	6571754443436630272	60,990 (3219)	7.54 (0.19)	0.53 (0.06)	H	270	5.74	1
2214–3740	DA	6598092346829714560	31,360 (560)	8.06 (0.09)	0.68 (0.05)	H	171	6.90	1
2227–3246	DO	6601723758858306304	49,700 (978)	8.01 (0.38)	0.65 (0.19)	He	305	6.36	

Table 2—Continued

MCT	Type	Gaia ID (EDR3)	T_{eff} (K)	$\log g$	M/M_{\odot}	Comp	$D(\text{pc})$	$\log \tau$	Notes
2231–2935	DA	6608413462479644928	17,280 (405)	8.20 (0.07)	0.73 (0.04)	H	—	8.26	5
2233–3529	DA	6597106153619823488	29,350 (535)	8.06 (0.08)	0.68 (0.04)	H	131	7.02	
2241–4031	DC	6545617505854472192	10,080 (141)	7.88 (0.03)	0.52 (0.01)	log H/He=−4.6	69	8.74	4
2251–6326	DA	6394241555306538240	18,940 (410)	7.92 (0.07)	0.57 (0.04)	H	46	7.84	1
2252–4042	DA+dM:	6546151898569986688	66,130 (2757)	7.85 (0.15)	0.65 (0.06)	H	911	5.95	
2259–2646	DA	2382502441666663168	19,620 (529)	7.82 (0.08)	0.53 (0.04)	H	74	7.67	1
2259–3212	DA+dM	6604630592725421440	85,710 (6686)	6.99 (0.21)	0.47 (0.05)	H	317	—	
2306–2726	DA	2379359556397873664	19,140 (715)	7.53 (0.12)	0.40 (0.04)	H	163	7.53	1
2311–2605	DA	2379935013296113664	45,480 (1933)	8.14 (0.18)	0.75 (0.10)	H	315	6.38	
2313–3303	DA+dM	6555925496084361344	41,560 (971)	7.41 (0.10)	0.44 (0.03)	H	463	5.76	
2318–2236	DA	2385336982642954496	31,110 (637)	7.89 (0.11)	0.59 (0.05)	H	185	6.90	
2322–1808	DA	2393546245693497728	22,130 (640)	7.76 (0.09)	0.51 (0.04)	H	93	7.39	
2326–2226	DA	2388347308040329216	21,100 (1033)	7.91 (0.15)	0.58 (0.08)	H	109	7.60	
2329–3317	DA	2325117757286653440	20,600 (668)	7.97 (0.10)	0.61 (0.06)	H	148	7.72	
2330–2113	DA	2388953031573382784	26,700 (517)	7.63 (0.07)	0.47 (0.03)	H	263	7.04	
2331–4731	DA	6528109879126984960	54,350 (1145)	7.74 (0.07)	0.58 (0.03)	H	106	6.17	1
2333–1634	DA	2395444208921491456	14,240 (607)	8.09 (0.07)	0.66 (0.04)	H	24	8.44	
2334–4127	DB	6537005065634429312	21,190 (994)	8.28 (0.09)	0.77 (0.06)	He	75	8.03	
2336–1842	DA	2393875961742886656	7710 (126)	7.39 (0.15)	0.31 (0.05)	H	37	8.79	3
2336–1955	DA	2390640129086674560	20,060 (328)	8.05 (0.05)	0.65 (0.03)	H	145	7.87	1
2343–1740	DA	2394370123500185344	22,460 (381)	8.12 (0.05)	0.70 (0.03)	H	165	7.72	1
2345–3940	DA	6534665545408513792	20,650 (328)	7.95 (0.05)	0.60 (0.03)	H	113	7.69	1
2347–1916	DA	2390888829168611968	27,600 (599)	7.86 (0.09)	0.57 (0.04)	H	150	7.07	1
2349–2819	DA	2334079090586541440	18,670 (478)	7.96 (0.08)	0.60 (0.04)	H	86	7.91	1
2349–3627	DA	2311200968031379584	51,490 (1124)	7.64 (0.08)	0.54 (0.03)	H	351	6.18	1
2350–2448	DA	2338275136195124864	30,560 (608)	8.41 (0.10)	0.89 (0.06)	H	87	7.43	1
2352–1249	DA	2421871039614828672	44,930 (1519)	8.00 (0.14)	0.68 (0.07)	H	444	6.42	1
2354–1510	DA	2419140746085234688	37,220 (605)	7.17 (0.06)	0.34 (0.02)	H	347	—	1, 3
2354–3033	DB	2326837707005769216	24,950 (2645)	7.98 (0.08)	0.60 (0.04)	He	156	7.32	1
2359–3228	DA	2313582750735435776	22,780 (372)	7.99 (0.05)	0.62 (0.03)	H	192	7.51	1

Note. — (1) Spectroscopically classified as a white dwarf in the MWDD; (2) ZZ Ceti variable; (3) Double degenerate binary candidate; (4) Physical parameters determined from the *Gaia* photometry and parallax; (5) No *Gaia* parallax available.

REFERENCES

- Barnett, J. W., Williams, K. A., Bédard, A., & Bolte, M. 2021, arXiv e-prints, arXiv:2107.06373
- Barstow, M. A., Hodgkin, S. T., Pye, J. P., King, A. R., Fleming, T. A., Holberg, J. B., & Tweedy, R. W. 1993, in NATO Advanced Study Institute (ASI) Series C, Vol. 403, White Dwarfs: Advances in Observation and Theory, ed. M. A. Barstow, 433
- Barstow, M. A., O’Donoghue, D., Kilkenney, D., Burleigh, M. R., & Fleming, T. A. 1995, MNRAS, 273, 711
- Bédard, A., Bergeron, P., Brassard, P., & Fontaine, G. 2020, ApJ, 901, 93
- Bergeron, P., Dufour, P., Fontaine, G., Coutu, S., Blouin, S., Genest-Beaulieu, C., Bédard, A., & Rolland, B. 2019, ApJ, 876, 67
- Bergeron, P., Ruiz, M. T., & Leggett, S. K. 1997, ApJS, 108, 339
- Bergeron, P., Saffer, R. A., & Liebert, J. 1992, ApJ, 394, 228
- Bergeron, P., Wesemael, F., Dufour, P., Beauchamp, A., Hunter, C., Saffer, R. A., Gianninas, A., Ruiz, M. T., Limoges, M.-M., Dufour, P., Fontaine, G., & Liebert, J. 2011, ApJ, 737, 28
- Bergeron, P., Wesemael, F., Lamontagne, R., Fontaine, G., Saffer, R. A., & Allard, N. F. 1995, ApJ, 449, 258
- Blouin, S., Dufour, P., Thibeault, C., & Allard, N. F. 2019, ApJ, 878, 63
- Coutu, S., Dufour, P., Bergeron, P., Blouin, S., Loranger, E., Allard, N. F., & Dunlap, B. H. 2019, ApJ, 885, 74
- Cristiani, S., La Franca, F., Andreani, P., Gemmo, A., Goldschmidt, P., Miller, L., Vio, R., Barbieri, C., Bodini, L., Iovino, A., Lazzarin, M., Clowes, R., MacGillivray, H., Gouiffes, C., Lissandrini, C., & Savage, A. 1995, A&AS, 112, 347
- Cukanovaite, E., Tremblay, P.-E., Bergeron, P., Freytag, B., Ludwig, H.-G., & Steffen, M. 2021, MNRAS, 501, 5274
- Demers, S., Beland, S., Kibblewhite, E. J., Irwin, M. J., & Nithakorn, D. S. 1986, AJ, 92, 878

- Demers, S., Wesemael, F., Irwin, M. J., Fontaine, G., Lamontagne, R., Kepler, S. O., & Holberg, J. B. 1990, *ApJ*, 351, 271
- Dufour, P., Blouin, S., Coutu, S., Fortin-Archambault, M., Thibeault, C., Bergeron, P., & Fontaine, G. 2017, in *Astronomical Society of the Pacific Conference Series*, Vol. 509, 20th European White Dwarf Workshop, ed. P.-E. Tremblay, B. Gaensicke, & T. Marsh, 3
- Feige, J. 1958, *ApJ*, 128, 267
- Gaia Collaboration, Babusiaux, C., van Leeuwen, F., Barstow, M. A., Jordi, C., Vallenari, A., Bossini, D., Bressan, A., Cantat-Gaudin, T., van Leeuwen, M., & et al. 2018, *A&A*, 616, A10
- Gaia Collaboration, Brown, A. G. A., Vallenari, A., Prusti, T., de Bruijne, J. H. J., Babusiaux, C., Biermann, M., Creevey, O. L., Evans, D. W., Eyer, L., Hutton, A., Jansen, F., Jordi, C., Klioner, S. A., Lammers, U., Lindegren, L., Luri, X., Mignard, F., Panem, C., Pourbaix, D., Randich, S., Sartoretti, P., Soubiran, C., Walton, N. A., Arenou, F., Bailer-Jones, C. A. L., Bastian, U., Cropper, M., Drimmel, R., Katz, D., Lattanzi, M. G., van Leeuwen, F., Bakker, J., Cacciari, C., Castañeda, J., De Angeli, F., Ducourant, C., Fabricius, C., Fouesneau, M., Frémat, Y., Guerra, R., Guerrier, A., Guiraud, J., Jean-Antoine Piccolo, A., Masana, E., Messineo, R., Mowlavi, N., Nicolas, C., Nienartowicz, K., Pailler, F., Panuzzo, P., Riclet, F., Roux, W., Seabroke, G. M., Sordo, R., Tanga, P., Thévenin, F., Gracia-Abril, G., Portell, J., Teyssier, D., Altmann, M., Andrae, R., Bellas-Velidis, I., Benson, K., Berthier, J., Blomme, R., Brugaletta, E., Burgess, P. W., Busso, G., Carry, B., Cellino, A., Cheek, N., Clementini, G., Damerджи, Y., Davidson, M., Delchambre, L., Dell’Oro, A., Fernández-Hernández, J., Galluccio, L., García-Lario, P., Garcia-Reinaldos, M., González-Núñez, J., Gosset, E., Haignon, R., Halbwegs, J. L., Hambly, N. C., Harrison, D. L., Hatzidimitriou, D., Heiter, U., Hernández, J., Hestroffer, D., Hodgkin, S. T., Holl, B., Janßen, K., Jevardat de Fombelle, G., Jordan, S., Krone-Martins, A., Lanzafame, A. C., Löffler, W., Lorca, A., Manteiga, M., Marchal, O., Marrese, P. M., Moitinho, A., Mora, A., Muinonen, K., Osborne, P., Pancino, E., Pauwels, T., Petit, J. M., Recio-Blanco, A., Richards, P. J., Riello, M., Rimoldini, L., Robin, A. C., Roegiers, T., Rybizki, J., Sarro, L. M., Siopis, C., Smith, M., Sozzetti, A., Ulla, A., Utrilla, E., van Leeuwen, M., van Reeven, W., Abbas, U., Abreu Aramburu, A., Accart, S., Aerts, C., Aguado, J. J., Ajaj, M., Altavilla, G., Álvarez, M. A., Álvarez Cid-Fuentes, J., Alves, J., Anderson, R. I., Anglada Varela, E., Antoja, T., Audard, M., Baines, D., Baker, S. G., Balaguer-Núñez, L., Balbinot, E., Balog, Z., Barache, C., Barbato, D., Barros, M., Barstow, M. A., Bartolomé, S., Bassilana, J. L.,

Bauchet, N., Baudesson-Stella, A., Becciani, U., Bellazzini, M., Bernet, M., Bertone, S., Bianchi, L., Blanco-Cuaresma, S., Boch, T., Bombrun, A., Bossini, D., Bouquillon, S., Bragaglia, A., Bramante, L., Breedt, E., Bressan, A., Brouillet, N., Bucciarelli, B., Burlacu, A., Busonero, D., Butkevich, A. G., Buzzi, R., Caffau, E., Cancelliere, R., Cánovas, H., Cantat-Gaudin, T., Carballo, R., Carlucci, T., Carnerero, M. I., Carrasco, J. M., Casamiquela, L., Castellani, M., Castro-Ginard, A., Castro Sampol, P., Chaoul, L., Charlot, P., Chemin, L., Chiavassa, A., Cioni, M. R. L., Comoretto, G., Cooper, W. J., Cornez, T., Cowell, S., Crifo, F., Crosta, M., Crowley, C., Dafonte, C., Dapergolas, A., David, M., David, P., de Laverny, P., De Luise, F., De March, R., De Ridder, J., de Souza, R., de Teodoro, P., de Torres, A., del Peloso, E. F., del Pozo, E., Delbo, M., Delgado, A., Delgado, H. E., Delisle, J. B., Di Matteo, P., Diakite, S., Diener, C., Distefano, E., Dolding, C., Eappachen, D., Edvardsson, B., Enke, H., Esquej, P., Fabre, C., Fabrizio, M., Faigler, S., Fedorets, G., Fernique, P., Fienga, A., Figueras, F., Fouron, C., Fragkoudi, F., Fraile, E., Franke, F., Gai, M., Garabato, D., Garcia-Gutierrez, A., García-Torres, M., Garofalo, A., Gavras, P., Gerlach, E., Geyer, R., Giacobbe, P., Gilmore, G., Girona, S., Giuffrida, G., Gomel, R., Gomez, A., Gonzalez-Santamaria, I., González-Vidal, J. J., Granvik, M., Gutiérrez-Sánchez, R., Guy, L. P., Hauser, M., Haywood, M., Helmi, A., Hidalgo, S. L., Hilger, T., Hładczuk, N., Hobbs, D., Holland, G., Huckle, H. E., Jasniewicz, G., Jonker, P. G., Juaristi Campillo, J., Julbe, F., Karbevská, L., Kervella, P., Khanna, S., Kochoska, A., Kontizas, M., Kordopatis, G., Korn, A. J., Kostrzewa-Rutkowska, Z., Kruszyńska, K., Lambert, S., Lanza, A. F., Lasne, Y., Le Champion, J. F., Le Fustec, Y., Lebreton, Y., Lebzelter, T., Leccia, S., Leclerc, N., Lecoœur-Taïbi, I., Liao, S., Licata, E., Lindstrøm, E. P., Lister, T. A., Livanou, E., Lobel, A., Madrero Pardo, P., Managau, S., Mann, R. G., Marchant, J. M., Marconi, M., Marcos Santos, M. M. S., Marinoni, S., Marocco, F., Marshall, D. J., Martin Polo, L., Martín-Fleitas, J. M., Masip, A., Massari, D., Mastrobuono-Battisti, A., Mazeh, T., McMillan, P. J., Messina, S., Michalik, D., Millar, N. R., Mints, A., Molina, D., Molinaro, R., Molnár, L., Montegriffo, P., Mor, R., Morbidelli, R., Morel, T., Morris, D., Mulone, A. F., Munoz, D., Muraveva, T., Murphy, C. P., Musella, I., Noval, L., Ordénovic, C., Orrù, G., Osinde, J., Pagani, C., Pagano, I., Palaversa, L., Palicio, P. A., Panahi, A., Pawlak, M., Peñalosa Esteller, X., Penttilä, A., Piersimoni, A. M., Pineau, F. X., Plachy, E., Plum, G., Poggio, E., Poretti, E., Poujoulet, E., Prša, A., Pulone, L., Racero, E., Ragaini, S., Rainer, M., Raiteri, C. M., Rambaux, N., Ramos, P., Ramos-Lerate, M., Re Fiorentin, P., Regibo, S., Reylé, C., Ripepi, V., Riva, A., Rixon, G., Robichon, N., Robin, C., Roelens, M., Rohrbasser, L., Romero-Gómez, M., Rowell, N., Royer, F., Rybicki, K. A., Sadowski, G., Sagristà Sellés, A., Sahlmann, J., Salgado, J., Salguero, E., Samaras, N., Sanchez Gimenez, V., Sanna, N., Santoveña, R., Sarasso, M., Schultheis, M., Sciacca, E., Segol,

- M., Segovia, J. C., Ségransan, D., Semeux, D., Shahaf, S., Siddiqui, H. I., Siebert, A., Siltala, L., Slezak, E., Smart, R. L., Solano, E., Solitro, F., Souami, D., Souchay, J., Spagna, A., Spoto, F., Steele, I. A., Steidelmüller, H., Stephenson, C. A., Süveges, M., Szabados, L., Szegedi-Elek, E., Taris, F., Tauran, G., Taylor, M. B., Teixeira, R., Thuillot, W., Tonello, N., Torra, F., Torra, J., Turon, C., Unger, N., Vaillant, M., van Dillen, E., Vanel, O., Vecchiato, A., Viala, Y., Vicente, D., Voutsinas, S., Weiler, M., Wevers, T., Wyrzykowski, L., Yoldas, A., Yvard, P., Zhao, H., Zorec, J., Zucker, S., Zurbach, C., & Zwitter, T. 2021, *A&A*, 649, A1
- Gemmo, A., La Franca, F., Cristiani, S., & Barbieri, C. 1993, in *NATO Advanced Study Institute (ASI) Series C, Vol. 403, White Dwarfs: Advances in Observation and Theory*, ed. M. A. Barstow, 23
- Gemmo, A. G., Cristiani, S., La Franca, F., & Andreani, P. 1995, in *White Dwarfs*, ed. D. Koester & K. Werner, Vol. 443, 31
- Genest-Beaulieu, C. & Bergeron, P. 2019, *ApJ*, 871, 169
- Gentile Fusillo, N. P., Tremblay, P.-E., Gänsicke, B. T., Manser, C. J., Cunningham, T., Cukanovaite, E., Hollands, M., Marsh, T., Raddi, R., Jordan, S., Toonen, S., Geier, S., Barstow, M., & Cummings, J. D. 2019, *MNRAS*, 482, 4570
- Gianninas, A., Bergeron, P., & Ruiz, M. T. 2011, *ApJ*, 743, 138
- Green, R. F., Schmidt, M., & Liebert, J. 1986, *ApJS*, 61, 305
- Haro, G. & Luyten, W. J. 1962, *Boletín de los Observatorios Tonantzintla y Tacubaya*, 3, 37
- Homeier, D., Koester, D., Hagen, H. J., Jordan, S., Heber, U., Engels, D., Reimers, D., & Dreizler, S. 1998, *A&A*, 338, 563
- Humason, M. L. & Zwicky, F. 1947, *ApJ*, 105, 85
- Kepler, S. O., Pelisoli, I., Koester, D., Reindl, N., Geier, S., Romero, A. D., Ourique, G., Oliveira, C. d. P., & Amaral, L. A. 2019, *MNRAS*, 486, 2169
- Kibblewhite, E. J., Bridgeland, M. T., Bunclark, P., & Irwin, M. 1984, in *NASA Conference Publication, Vol. 2317, NASA Conference Publication*, 277–288
- Kilic, M., Bergeron, P., Kosakowski, A., Brown, W. R., Agüeros, M. A., & Blouin, S. 2020, *ApJ*, 898, 84

- Kondo, M., Noguchi, T., & Maehara, H. 1984, *Annals of the Tokyo Astronomical Observatory*, 20, 130
- Lamontagne, R., Demers, S., Wesemael, F., Fontaine, G., & Irwin, M. J. 2000, *AJ*, 119, 241
- Lanning, H. H. 1973, *PASP*, 85, 70
- Liebert, J., Bergeron, P., & Holberg, J. B. 2005, *ApJS*, 156, 47
- Lindegren, L., Klioner, S. A., Hernández, J., Bombrun, A., Ramos-Lerate, M., Steidelmüller, H., Bastian, U., Biermann, M., de Torres, A., Gerlach, E., Geyer, R., Hilger, T., Hobbs, D., Lammers, U., McMillan, P. J., Stephenson, C. A., Castañeda, J., Davidson, M., Fabricius, C., Gracia-Abril, G., Portell, J., Rowell, N., Teyssier, D., Torra, F., Bartolomé, S., Clotet, M., Garralda, N., González-Vidal, J. J., Torra, J., Abbas, U., Altmann, M., Anglada Varela, E., Balaguer-Núñez, L., Balog, Z., Barache, C., Becciani, U., Bernet, M., Bertone, S., Bianchi, L., Bouquillon, S., Brown, A. G. A., Bucciarelli, B., Busonero, D., Butkevich, A. G., Buzzi, R., Cancelliere, R., Carlucci, T., Charlot, P., Cioni, M. R. L., Crosta, M., Crowley, C., del Peloso, E. F., del Pozo, E., Drimmel, R., Esquej, P., Fienga, A., Fraile, E., Gai, M., Garcia-Reinaldos, M., Guerra, R., Hambly, N. C., Hauser, M., Janßen, K., Jordan, S., Kostrzewa-Rutkowska, Z., Lattanzi, M. G., Liao, S., Licata, E., Lister, T. A., Löffler, W., Marchant, J. M., Masip, A., Mignard, F., Mints, A., Molina, D., Mora, A., Morbidelli, R., Murphy, C. P., Pagani, C., Panuzzo, P., Peñalosa Esteller, X., Poggio, E., Re Fiorentin, P., Riva, A., Sagristà Sellés, A., Sanchez Gimenez, V., Sarasso, M., Sciacca, E., Siddiqui, H. I., Smart, R. L., Souami, D., Spagna, A., Steele, I. A., Taris, F., Utrilla, E., van Reeven, W., & Vecchiato, A. 2021, *A&A*, 649, A2
- McCook, G. P. & Sion, E. M. 1999, *ApJS*, 121, 1
- Noguchi, T., Maehara, H., & Kondo, M. 1980, *Annals of the Tokyo Astronomical Observatory*, 18, 55
- Reimers, D., Jordan, S., Beckmann, V., Christlieb, N., & Wisotzki, L. 1998, *A&A*, 337, L13
- Reimers, D., Jordan, S., Koester, D., Bade, N., Koehler, T., & Wisotzki, L. 1996, *A&A*, 311, 572
- Reindl, N., Bainbridge, M., Przybilla, N., Geier, S., Prvák, M., Krtička, J., Østensen, R. H., Telting, J., & Werner, K. 2019, *MNRAS*, 482, L93
- Reindl, N., Schaffenroth, V., Filiz, S., Geier, S., Pelisoli, I., & Kepler, S. O. 2021, *A&A*, 647, A184

- Rolland, B., Bergeron, P., & Fontaine, G. 2018, *ApJ*, 857, 56
- Stobie, R. S., Chen, A., O’Donoghue, D., & Kilkenny, D. 1992, in *Astronomical Society of the Pacific Conference Series*, Vol. 30, *Variable Stars and Galaxies*, in honor of M. W. Feast on his retirement, ed. B. Warner, 87
- Stobie, R. S., Kilkenny, D., Koen, C., & O’Donoghue, D. 1997, in *The Third Conference on Faint Blue Stars*, ed. A. G. D. Philip, J. Liebert, R. Saffer, & D. S. Hayes, 497
- Stobie, R. S., Morgan, D. H., Bhatia, R. K., Kilkenny, D., & O’Donoghue, D. 1987, in *IAU Colloq. 95: Second Conference on Faint Blue Stars*, ed. A. G. D. Philip, D. S. Hayes, & J. W. Liebert, 493–496
- Tremblay, P.-E., Bergeron, P., & Gianninas, A. 2011a, *ApJ*, 730, 128
- Tremblay, P. E., Bergeron, P., Kalirai, J. S., & Gianninas, A. 2010, *ApJ*, 712, 1345
- Tremblay, P. E., Hollands, M. A., Gentile Fusillo, N. P., McCleery, J., Izquierdo, P., Gänsicke, B. T., Cukanovaite, E., Koester, D., Brown, W. R., Charpinet, S., Cunningham, T., Farihi, J., Giammichele, N., van Grootel, V., Hermes, J. J., Hoskin, M. J., Jordan, S., Kepler, S. O., Kleinman, S. J., Manser, C. J., Marsh, T. R., de Martino, D., Nitta, A., Parsons, S. G., Pelisoli, I., Raddi, R., Rebassa-Mansergas, A., Ren, J. J., Schreiber, M. R., Silvotti, R., Toloza, O., Toonen, S., & Torres, S. 2020, *MNRAS*, 497, 130
- Tremblay, P. E., Ludwig, H. G., Steffen, M., Bergeron, P., & Freytag, B. 2011b, *A&A*, 531, L19
- Tremblay, P.-E., Ludwig, H.-G., Steffen, M., & Freytag, B. 2013, *A&A*, 552, A13
- Wagner, R. M., Sion, E. M., Liebert, J., & Starrfield, S. G. 1988, *ApJ*, 328, 213
- Wesemael, F., Bergeron, P., Lamontagne, R. L., Fontaine, G., Beauchamp, A., Demers, S., Irwin, M. J., Holberg, J. B., Kepler, S. O., & Vennes, S. 1994, *ApJ*, 429, 369